Lithos 240–243 (2016) 382–401

Contents lists available at ScienceDirect

Lithos

journal homepage: www.elsevier.com/locate/lithos

Different sources involved in generation of continental arc volcanism: The Carboniferous–Permian volcanic rocks in the northern margin of the North China block

Shuan-Hong Zhang [a,b,*], Yue Zhao [a], Jian-Min Liu [a], Zhao-Chu Hu [b]

[a] Institute of Geomechanics, Chinese Academy of Geological Sciences, MLR Key Laboratory of Paleomagnetism and Tectonic Reconstruction, Beijing 100081, China
[b] State Key Laboratory of Geological Processes and Mineral Resources, China University of Geosciences, Wuhan 430074, China

ARTICLE INFO

Article history:
Received 3 June 2015
Accepted 8 November 2015
Available online 7 December 2015

Keywords:
Andean-type continental margin
Continental arc magmatism
MASH zone
Magma homogenization
North China block (NCB)
Central Asian Orogenic Belt (CAOB)

ABSTRACT

New zircon U–Pb dating results on the Carboniferous–Permian volcanic rocks in the northern margin of the North China block (NCB) indicate their eruption during the Early Carboniferous to Late Permian from 347 ± 3 Ma to 258 ± 1 Ma and a slight decrease of the upper limits of the volcanic sequences from west to east. They have a main rock association of basalt, basaltic andesite, andesite, dacite, rhyolite, tuff, and tufaceous sandstone. Most of them have calc-alkaline compositions and exhibit variable SiO_2 contents from 48.2 wt.% to 77.1 wt.%. There is no significant gap between the mafic and felsic volcanic rocks in major and trace element classification diagrams, indicating that they are not bimodal in composition. The Carboniferous–Permian volcanic rocks exhibit subduction-related geochemical features such as negative Nb and Ta anomalies of mafic to intermediate rocks on primitive mantle-normalized diagrams, indicating they were formed in an Andean-type continental arc during southward subduction of the Paleo-Asian oceanic plate beneath the northern NCB. However, their wide range of whole-rock Sr–Nd and zircon Hf isotopic compositions indicate that their source areas are very complex and different sources were involved in generation of these volcanic rocks. Geochemical and Sr–Nd–Hf isotopic results show that the basalt and some andesite were produced by fractional crystallization of mafic magma derived from partial melting of mantle wedge and subducted oceanic crust; however, most of the intermediate to felsic volcanic rocks were derived from partial melting of lower continental crust. There is an increasing input of crustal materials from the Carboniferous to Permian as indicated by increasing volumes of felsic volcanic rocks in the volcanic sequences. The results show that origin of the continental arc volcanism is very complex and both materials from the subducted oceanic crust and sediments, mantle wedge and arc continental crust could be involved in their generation. For the Permian andesite, dacite and rhyolitic volcanic rocks, there is a striking correlation between their Sr–Nd–Hf isotopic compositions and those of the underlying basement. Sr–Nd–Hf isotopic differences between the Permian intermediate to felsic volcanic rocks from either side of the northern boundary fault of the North China craton suggest that mixture and homogenization of the magmas in the melting–assimilation–storage–hybridization (MASH) zone within this continental arc was incomplete, and incomplete homogenization of magmas is likely a common feature of many MASH zones within continental arcs. Our results on the volcanic rocks also show that the final closure of the Paleo-Asian Ocean along the Solonker Suture Zone has not been finished prior to the Middle Permian and the decease of the Paleo-Asian oceanic subduction beneath the northern NCB in its middle-western parts is a little earlier than that in its eastern part.

1. Introduction

Continental arcs, such as the Andean arc of South America, represent the product of subduction magmatism where the upper plate is continental and/or accreted transitional lithosphere (Ducea et al., 2015). In contrast to the oceanic crust that is basaltic (~50 wt.% SiO_2) in composition, the bulk continental crust is andesitic (~60 wt.% SiO_2) in composition (e.g., Jagoutz and Kelemen, 2015; Rudnick, 1995; Rudnick and Gao, 2003; Taylor and McLennan, 1985), and continental arcs therefore are Earth's largest sites of intermediate magmatism (e.g., Ducea et al., 2015). Thus, the magmatic mechanisms operating in continental arcs contain another layer of complexity compared with those in oceanic island arcs (e.g., Ducea et al., 2015; Jagoutz and Kelemen, 2015). Therefore, unraveling continental arc evolution from petrologic, geochemical, and tectonic perspectives is challenging and has great significance for understanding the formation and evolution of continental crust and mechanisms for generating large volumes of intermediate magmas (e.g., Ducea et al., 2015).

* Corresponding author at: No. 11 South Minzudaxue Road, Haidian District, Beijing 100081, China. Tel.: +86 10 88815058; fax: +86 10 68422326.
E-mail address: tozhangshuanhong@163.com (S.-H. Zhang).

http://dx.doi.org/10.1016/j.lithos.2015.11.027
0024-4937/

The northern margin of the North China block (NCB), which serves as part of the southern boundary of the Central Asian Orogenic Belt (CAOB, Jahn et al., 2000 or Altaids, Sengör et al., 1993), was previously regarded as a passive continental margin during the Late Paleozoic period (e.g., Hsu et al., 1991; Robinson et al., 1999). However, in recent years many Late Carboniferous to Permian granitoid intrusions had been recognized from what were regarded previously as Archean to Paleoproterozoic lithological assemblages in the northern NCB (e.g., Wang et al., 2007; Zhang et al., 2004, 2007a, 2009a,b). They are calc-alkaline or high-K calc-alkaline, metaluminous or weak peraluminous, and were considered to reflect arc magmatism along an Andean-type continental margin (e.g., Bai et al., 2013; Li, 2006; Ma et al., 2013; Wang and Liu, 1986; Wang et al., 2007; Xiao et al., 2003, 2009; Zhang and Zhao, 2013; Zhang et al., 2007a, 2009a,b).

Prior to its evolution into a continental arc, the northern margin of NCB was laterally accreted by arc-continent collision during the Late Silurian to earliest Devonian period, leading to accretion of the Bainaimiao arc to the northern margin of the North China craton (NCC), reversal of arc polarity and transitions of the northern NCC from a passive to active continental margin (Zhang et al., 2014). The accreted Bainaimiao arc along the northern margin of NCB in the upper plate of the subduction zone is characterized by different architecture and composition than the NCC (Zhang et al., 2014). Therefore, the northern margin of the NCB provides an excellent area to study the complex processes and different sources involved in generation of continental arc volcanism.

2. Geological setting and previous studies

The northern NCB consists mainly of two tectonic units including the NCC and the Bainaimiao arc belt, which are separated by the E–W-trending Bayan Obo–Duolun–Chifeng–Kaiyuan fault zone (Fig. 1). The basement of the NCC is composed of highly metamorphosed Archean and Paleoproterozoic rocks, which were covered by the Mesoproterozoic to Ordovician marine clastic and carbonate platformal sediments, Middle Carboniferous to Triassic fluvial and deltaic sediments, and Jurassic–Cretaceous and younger volcanic and sedimentary rocks. The Early Paleozoic Bainaimiao arc belt was built upon a Precambrian microcontinent that has a tectonic affinity to the Tarim or Yangtze cratons and was accreted to the northern NCC during the Late Silurian–earliest Devonian by arc-continent collision (Zhang et al., 2014). As shown in Fig. 1B, Carboniferous–Permian magmatic rocks are widely distributed in the northern margin of the NCB. However, in contrast to the intrusive rocks, the volcanic rocks are limited to areas near the boundary fault between the NCC and the Bainaimiao arc belt. Previous results (Liu et al., 2012; Ye et al., 2014; Zhang et al., 2006, 2007b) show that the Carboniferous–Permian volcanic rocks were likely widely distributed in the Inner Mongolia Paleo-uplift along the northern margin of the NCC; however, most of them have been eroded by Carboniferous–Early Jurassic uplift and exhumation. The tuff layers within the Carboniferous–Permian coal-bearing sedimentary rocks in the northern North China basins are additional records of the eroded arc volcanic rocks in the Inner Mongolia Paleo-uplift (Zhang et al., 2007b).

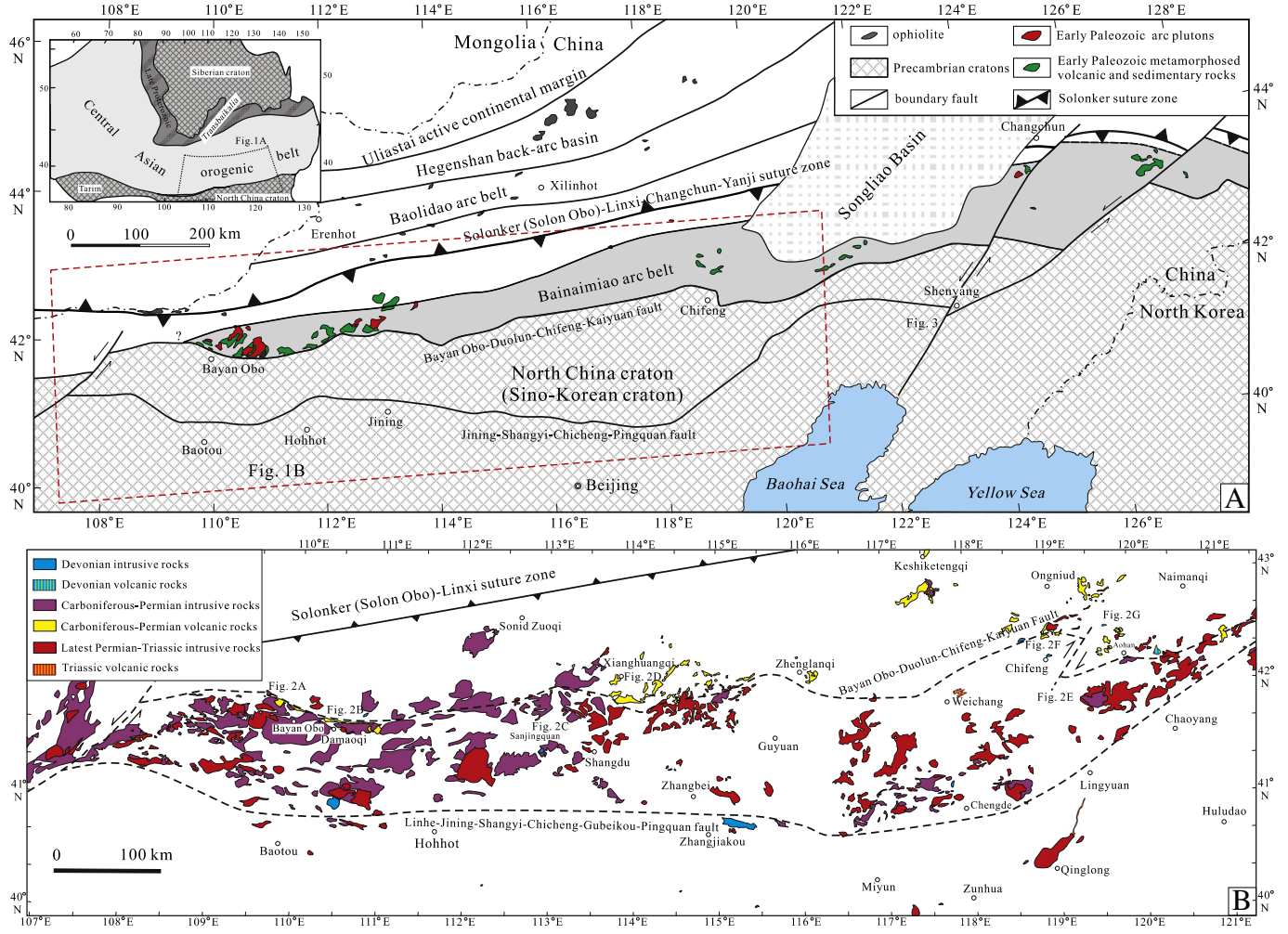

Fig. 1. (A) Sketch tectonic map of the southern CAOB and the northern margin of the NCB (modified after Zhang et al., 2014; inset figure is modified after Jahn et al., 2000); (B) Sketch map showing distribution of the Late Paleozoic to Early Mesozoic magmatic rocks in the northern NCB (modified after Zhang et al., 2010).

Although many results have been published on the Carboniferous–Permian intrusive rocks (e.g., Bai et al., 2013; Feng et al., 2009; Luo et al., 2009; Ma et al., 2013; Wang et al., 2007, 2009; Zhang and Zhao, 2013; Zhang et al., 2004, 2006, 2007a, 2009a,b,c, 2010, 2011a, 2012; Zhou et al., 2009), not much work has been conducted on the Carboniferous–Permian volcanic rocks in the northern NCB. Therefore, their ages and origin are still poorly understood. In contrast to the Carboniferous–Permian volcanic rocks north to the Solonker suture zone that are bimodal in composition (e.g., Zhang et al., 2008, 2011b) and were likely related to back-arc extension during northward subduction of the Paleo-Asian oceanic plate beneath the southern Mongolia composite terranes (e.g., Miao et al., 2008), the Carboniferous–Permian volcanic rocks in the northern NCB are mainly andesites in composition and exhibit rock associations of continental arc volcanism. Therefore, research on these volcanic rocks will provide important constraints on volcanic processes and the role of subducted slab, mantle wedge and continental crust in generation of the continental arc volcanism in the northern NCB.

3. Field occurrence and petrology of the Carboniferous–Permian volcanic rocks

The Carboniferous–Permian volcanic rocks in the northern NCB are especially common in areas such as Chifeng-Aohan, Xianghuangqi, Sanjingquan, Damaoqi and Bayan Obo (Figs. 1B and 2). They are composed mainly of basalt, basaltic andesite, andesite, dacite, rhyolite, tuff, tufaceous sandstone and minor hypabyssal rocks such as rhyolitic porphyry (Figs. 2–4). Although they were previously considered as

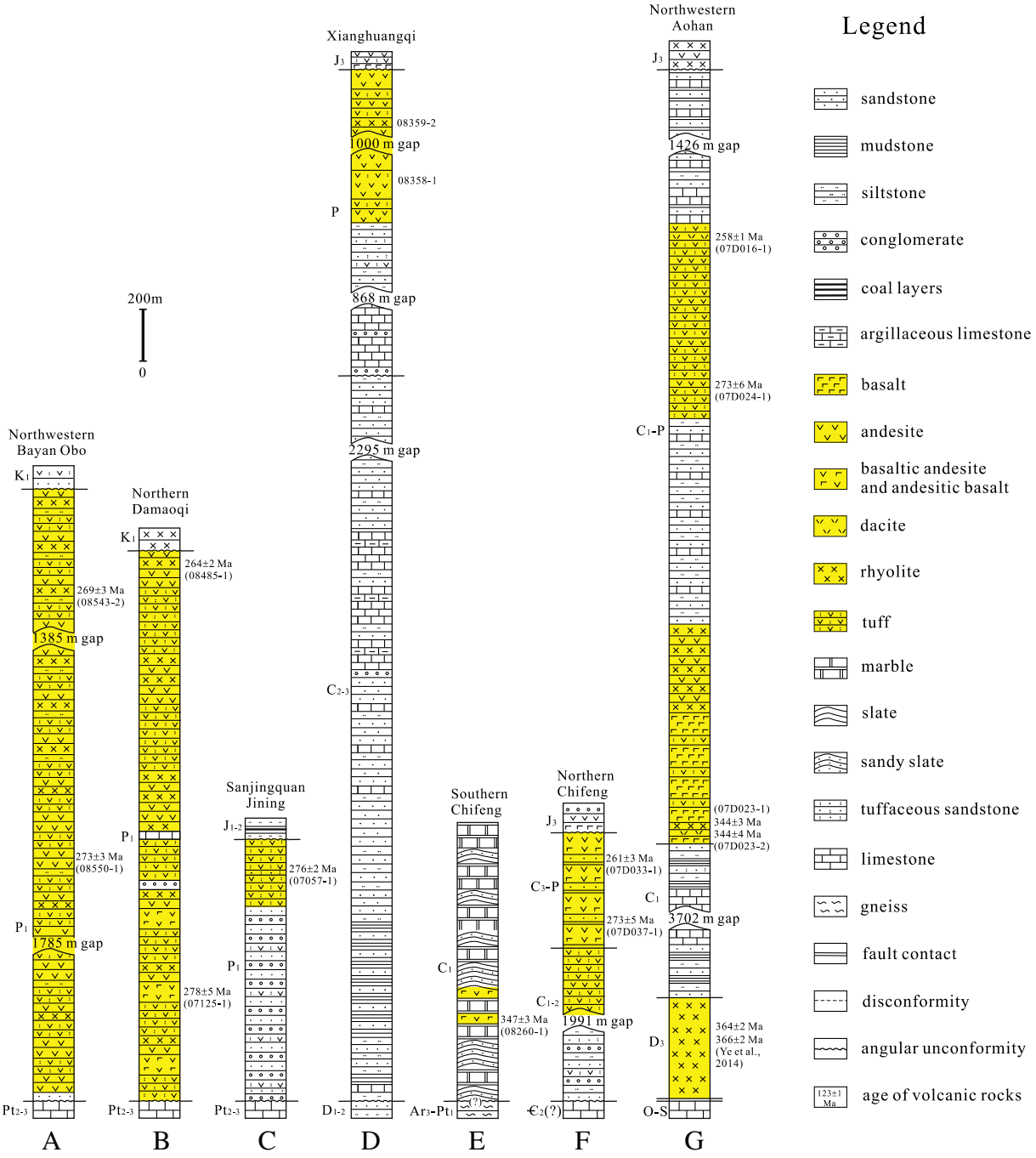

Fig. 2. Stratigraphic columns of Late Paleozoic volcanic and sedimentary rocks in the northern margin of the NCB. Locations of stratigraphic columns are marked in Fig. 1B.

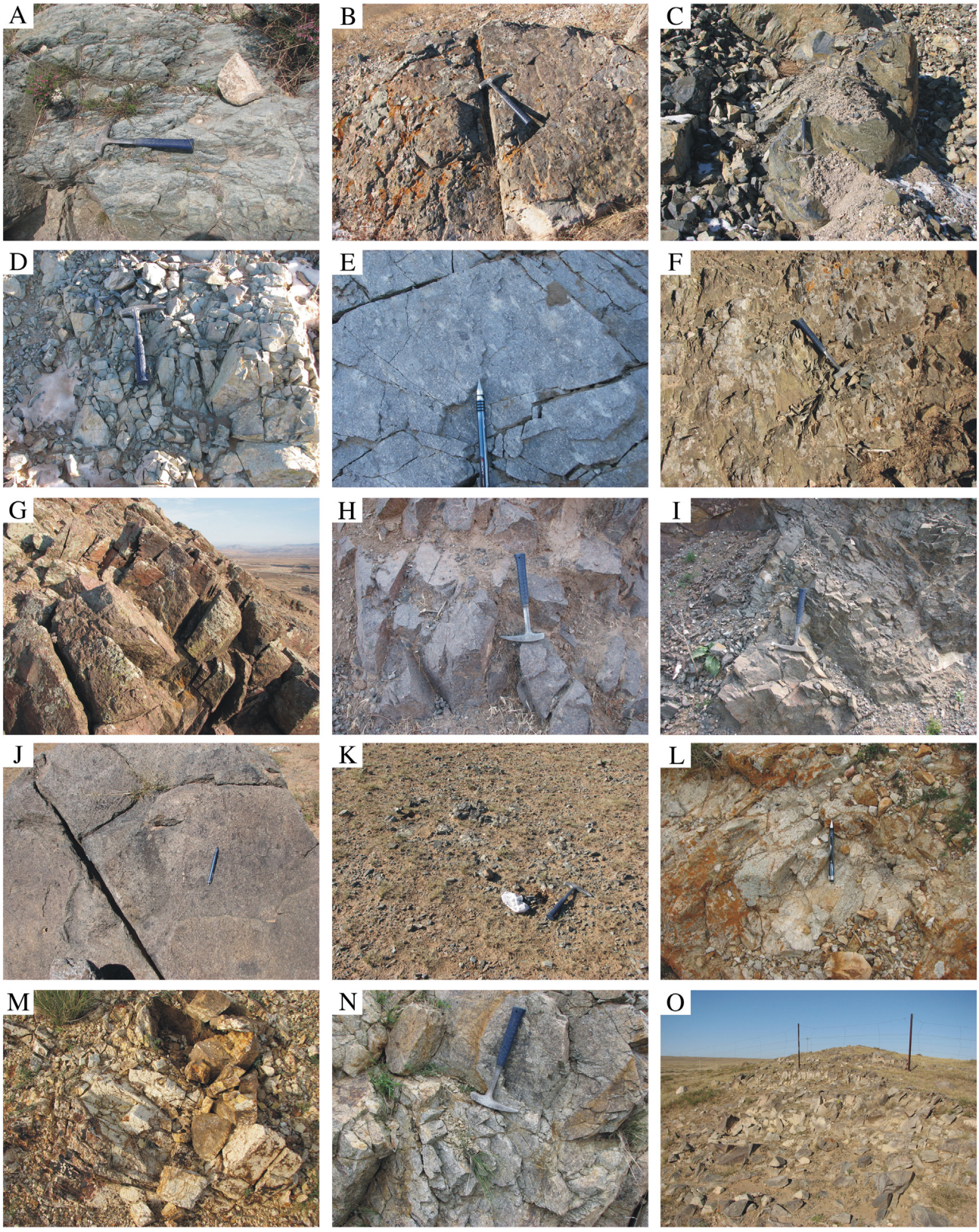

Fig. 3. Representative outcrop photos of the Carboniferous–Permian volcanic rocks in the northern margin of the NCB. (A) Early Carboniferous andesitic basalt near Louzidian, southern Chifeng (42°00.85′N, 119°01.24′E); (B) Early Carboniferous brecciated rhyolite from northwestern Aohan (42°24.16′N, 119°41.76′E); (C) Permian basalt from northwestern Aohan (42°25.76′N, 119°40.96′E); (D) Permian andesite from northwestern Aohan (42°24.40′N, 119°41.58′E); (E) Permian andesitic tuff from northwestern Aohan (42°24.16′N, 119°43.09′E); (F) Permian tuffaceous schist from northern Chifeng (42°33.43′N, 118°57.08′E); (G) Permian rhyolitic tuff from northern Chifeng (42°37.52′N, 118°38.40′E); (H) Permian andesite from northern Chifeng (42°37.76′N, 118°38.77′E); (I) Permian basaltic andesite from Xianghuangqi (42°01.17′N, 113°51.27′E); (J) Permian rhyolitic tuff from Sanjingquan (41°50.62′N, 112°51.18′E); (K) Permian basaltic andesite from northern Damaoqi (41°46.11′N, 110°32.64′E); (L) Permian rhyolite from northeastern Damaoqi (41°45.88′N, 110°43.92′E); (M) Permian rhyolite from northern Byan Obo (41°50.61′N, 110°07.99′E); (N) Permian andesite from northwestern Byan Obo (41°52.96′N, 109°59.24′E); (O) Permian rhyolitic porphyry near Chaganaobao Sumu, northern Damaoqi (41°56.73′N, 110°45.99′E).

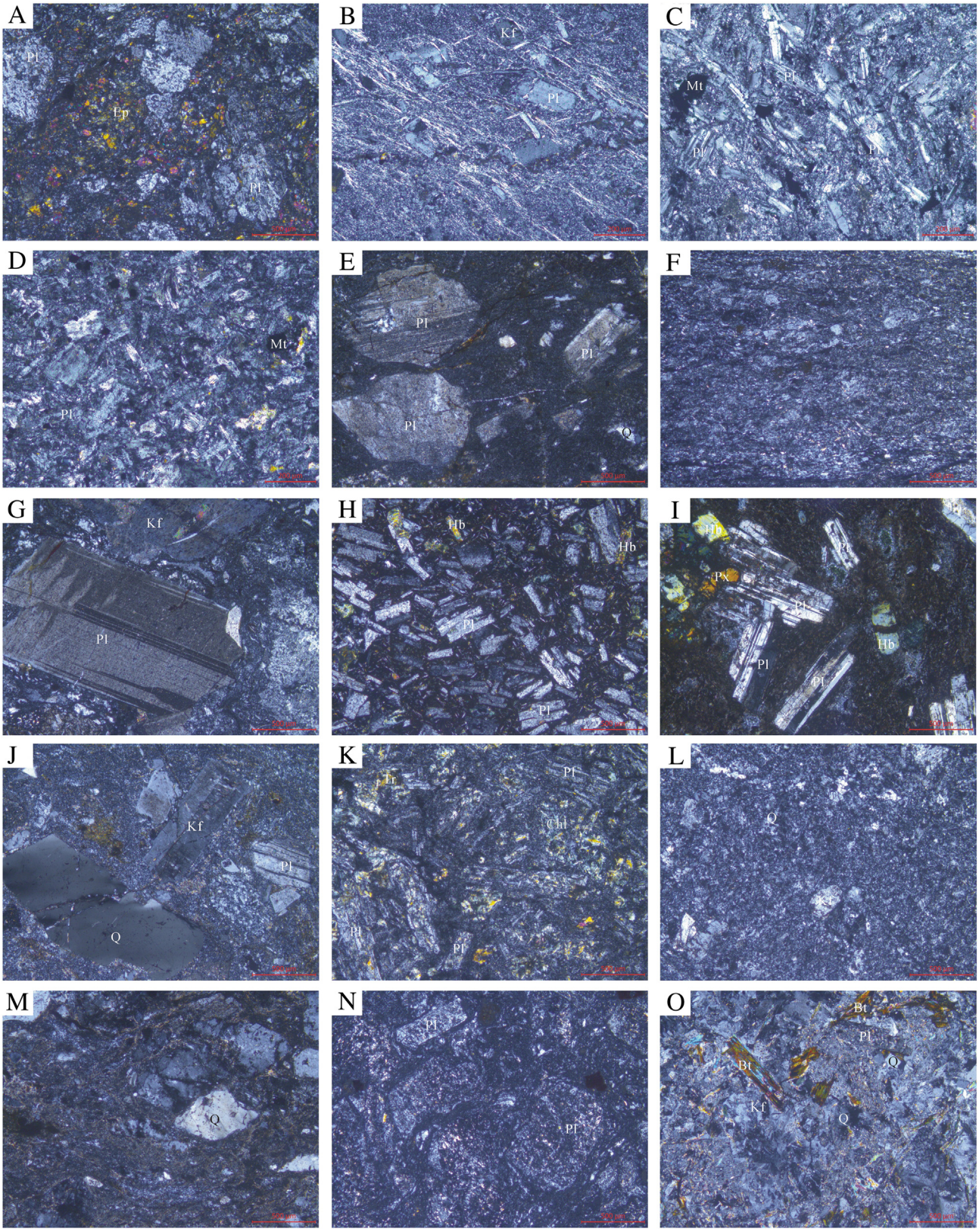

Fig. 4. Representative microphotographs (cross-polarized light) of the Carboniferous–Permian volcanic rocks in the northern margin of the NCB. (A) Early Carboniferous andesitic basalt (08260-1) near Louzidian, southern Chifeng; (B) Early Carboniferous brecciated rhyolite (07D023-1) from northwestern Aohan; (C) Permian basalt (07D025-1) from northwestern Aohan; (D) Permian andesite (07D024-1) from northwestern Aohan; (E) Permian dacite (07D016-1) from northwestern Aohan; (F) Permian tuffaceous schist (07D033-1) from northern Chifeng; (G) Permian rhyolitic tuff (07D037-1) from northern Chifeng; (H) Permian andesite (07D040-1) from northern Chifeng; (I) Permian basaltic andesite (08359-2) from Xianghuangqi; (J) Permian rhyolitic tuff (07058-1) from Sanjingquan; (K) Permian basaltic andesite (07125-1) from northern Damaoqi; (L) Permian rhyolite (08485-1) from northeastern Damaoqi; (M) Permian rhyolite (08549-1) from northern Byan Obo; (N) Permian andesite (08550-1) from northwestern Byan Obo; (O) Permian rhyolitic porphyry (07116-1) near Chaganaobao Sumu, northern Damaoqi. Mineral abbreviations: Px, pyroxene; Hb, hornblende; Bt, biotite; Pl, plagioclase; Q, quartz; Kf, K-feldspar; Mt, magnetite; Ep, epidote; Tr, tremolite; Chl, chlorite; Ser, sericite.

Carboniferous–Permian in ages (e.g., BGMRIM, 1967, 1970, 1971a,b, 1972, 1976, 1991; BGMRLP, 1971), no precise ages have been reported. Field occurrence and petrology of samples of the Carboniferous–Permian volcanic rocks in typical areas studied in this presentation are described below.

3.1. Chifeng–Aohan

The Carboniferous–Permian volcanic rocks in the Chifeng–Aohan area are about 2000 m thick and consist mainly of basalt, andesitic basalt, basaltic andesite, andesite, dacite, rhyolite, tuff, tuff breccia and tufaceous sandstone (Figs. 2E–G, 3A–H and 4A–H). They are widely distributed in northern Chifeng, northwestern Aohan, Keshiketengqi and eastern Ongniud (Fig. 1B). They were named as Qingfengshan Formation and were considered as Early Permian (e.g., BGMRIM, 1970; BGMRLP, 1971) or Carboniferous–Permian in age (e.g., BGMRIM, 1967). Some andesitic basalts interlayered with marbles and sandy slates near Louzidian (Figs. 1B, 2E, 3A and 4A), which were previously considered as Ordovician–Early Silurian (BGMRIM, 1967) or Late Cambrian (BGMRIM, 1970) in age, were proved to be Early Carboniferous in age in this study.

Sixteen samples from different layers of the volcanic sequences at several locations in the Chifeng–Aohan were collected for geochronological and geochemical studies. Among them sample 08260-1 is an andesitic basalt collected near Louzidian area south to Chifeng (Figs. 2E and 4A). Sample 07D023-1 is a brecciated rhyolite collected from the lower part of the volcanic sequences near Zhangjiayingzi northwest to Aohan (Figs. 2G and 4B). Samples 07D023-2 and 07D023-3 were collected from a similar location as 07D023-1 and their rock types are brecciated dacite and dacite, respectively. Sample 08197-1 is a rhyolitic tuffaceous schist collected near the Xar Moron River north to Chifeng. Sample 07D016-1 is a dacite collected from the upper part of the volcanic sequences near Halagou northwest to Aohan (Figs. 2G and 4E). Sample 07D020-1 is an andesite collected from the middle-upper part of the volcanic sequences near Tangshuiquan northwest to Aohan. Sample 07D024-1 is an andesite collected near Zhangjiayingzi northwest to Aohan (Figs. 2G and 4D). Sample 07D025-1 (Fig. 4C) and 07D028-1 are basalts collected from Zhangjiayingzi northwest to Aohan and Xialongfenggou north to Chifeng, respectively. Sample 07D033-1 is a dacitic tuffaceous schist collected near Xiaowudetu north to Chifeng (Figs. 2F and 4F). Sample 07D037-1 is a rhyolitic tuff collected near Dingjiawopu northwest to Chifeng (Figs. 2F and 4G). Sample 07D040-1 is an andesite collected near Gangzi northwest to Chifeng. Sample 07D041-1 is a rhyolite collected near Gangzi northwest to Chifeng (Fig. 4H). 07D043-1 and 07D043-2 are two basalt samples collected near Gangzi northwest to Chifeng.

3.2. Xianghuangqi

The Carboniferous–Permian volcanic rocks are very common in the Xianghuangqi area with a thickness over 1500 m (Figs. 2D, 3I and 4I). They were termed as Elitu or Sanmianjing Formations and consist of andesite, dacite, rhyolitic tuff, andesitic tuff and tufaceous sandstone. They were previously considered as Late Permian in age (BGMRIM, 1976).

Two samples were collected from the volcanic rocks in the Xianghuangqi area for geochronological and geochemical studies. Sample 08358-1 is a rhyolitic tuff collected near Haojiadi south to Xianghuangqi (Fig. 2D). Sample 08359-2 is a basaltic andesite collected near Haojiadi south to Xianghuangqi (Figs. 2D, 3I and 4I). Although we try to separate zircons from the above two samples, no sufficient zircons have been obtained for U–Pb dating.

3.2.1. Sanjingquan, Siziwangqi

The Carboniferous–Permian volcanic rocks near the Sanjingquan, Siziwangqi are distributed in a small outcrop area of 4 km^2. They are composed of rhyolitic tuff and tufaceous sandstone with thickness of 260 m (Figs. 2C, 3J and 4J). They were considered as Late Carboniferous to Early Permian in age (BGMRIM, 1972).

Two samples were collected for geochronological and geochemical studies. Samples 07057-1 and 07058-1 are two rhyolitic tuffs collected from the volcanic sequence in Sanjingquan, northeast Siziwangqi (Figs. 2C, 3J and 4J).

3.3. Damaoqi–Bayan Obo

The Carboniferous–Permian volcanic rocks in the Damaoqi–Bayan Obo areas are mainly distributed near the Walanbulage fault (Fig. 1B) which serves as the northern boundary fault of the NCC. They were termed as Baoligemiao Formation and assigned a Late Carboniferous age (BGMRIM, 1971a,b) or Suji Formation that is Early Permian in age (IMIGS, 2003). They consist mainly of andesite, andesitic volcanic breccia, dacite, rhyolite, rhyolitic porphyry and tufaceous sandstone (Figs. 2A–B, 3K–O and 4K–O). Thickness of the whole Carboniferous–Permian volcanic sequences ranges from 1000 to 5000 m (BGMRIM, 1971a,b; IMIGS, 2003). In Chaganaobao Sumu north east to Damaoqi, some rhyolitic porphyries have been found in the Ordovician–Silurian metamorphic sedimentary and intrusive rocks (Fig. 3O).

Seven samples from the volcanic sequence in the Damaoqi–Bayan Obo area were collected for geochronological and geochemical studies. Sample 07125-1 is a basaltic andesite collected near Huxiye northeast to Damaoqi (Figs. 2B and 4K). Samples 08485-1 and 08543-2 are two rhyolites collected near Baiyanhua northeast to Damaoqi and Bayinaobao Sum northwest to Damaoqi, respectively (Figs. 2A–B and 4L). Sample 08549-1 is a rhyolite collected near Agui northeast to Bayan Obo (Fig. 4M). Sample 08550-1 is an andesite collected near Agui northeast to Bayan Obo (Figs. 2A and 4N). Samples 07116-1 and 07117-1 are two rhyolitic porphyries collected from Chaganaobao Sumu northeast to Damaoqi (Fig. 4O).

4. Results

4.1. Zircon U–Pb geochronology

Fifteen samples including 8 from Chifeng–Aohan, 1 from Sanjingquan, Siziwangqi and 6 from Bayan Obo–Damaoqi were analyzed by SHRIMP or LA–ICP–MS U–Pb methods. The results are listed in Supplementary Tables A1 and A2 in the Electronic Supplementary Material (ESM) and are plotted in Fig. 6. A summary of zircon U–Pb ages of the Carboniferous–Permian volcanic rocks in the northern margin of the NCB is listed in Table 1. The ages and sample numbers are also marked in the stratigraphic columns in Fig. 2. Samples from Chifeng–Aohan yield eruption ages from 347 ± 3 Ma to 258 ± 1 Ma. Sample from Sanjingquan yields an eruption age of 276 ± 2 Ma. Samples from Bayan Obo–Damaoqi yield eruption ages from 278 ± 5 Ma to 261 ± 3 Ma. For volcanic rock samples from the Xianghuangqi area, no sufficient zircons have been obtained for U–Pb dating. However, the fusulinid and coral fossils identified from the limestone interbedded indicate that they are Early–Middle Permian in age.

4.2. Major and trace element compositions

Major and trace element compositions of 27 samples from the Carboniferous–Permian volcanic rocks in the northern margin of the NCB are listed in Supplementary Table A3 in the ESM. They exhibit a wide range of SiO_2 contents from 48.2 wt.% to 77.1 wt.%. In the total alkali (K_2O+Na_2O) vs. silica (SiO_2) classification diagram (Fig. 7A), most of them fall into the fields of basalt, basaltic andesite, basaltic trachyandesite, trachyandesite, trachydacite, dacite and rhyolite. In the K_2O vs. SiO_2 diagram (Fig. 7B), most of them fall into the fields of calc-alkaline and high-K calc-alkaline series. In Nb/Y vs. Zr/TiO_2 classification diagram (Fig. 7C) for volcanic rocks from Winchester and Floyd (1977), they are classified as subalkaline

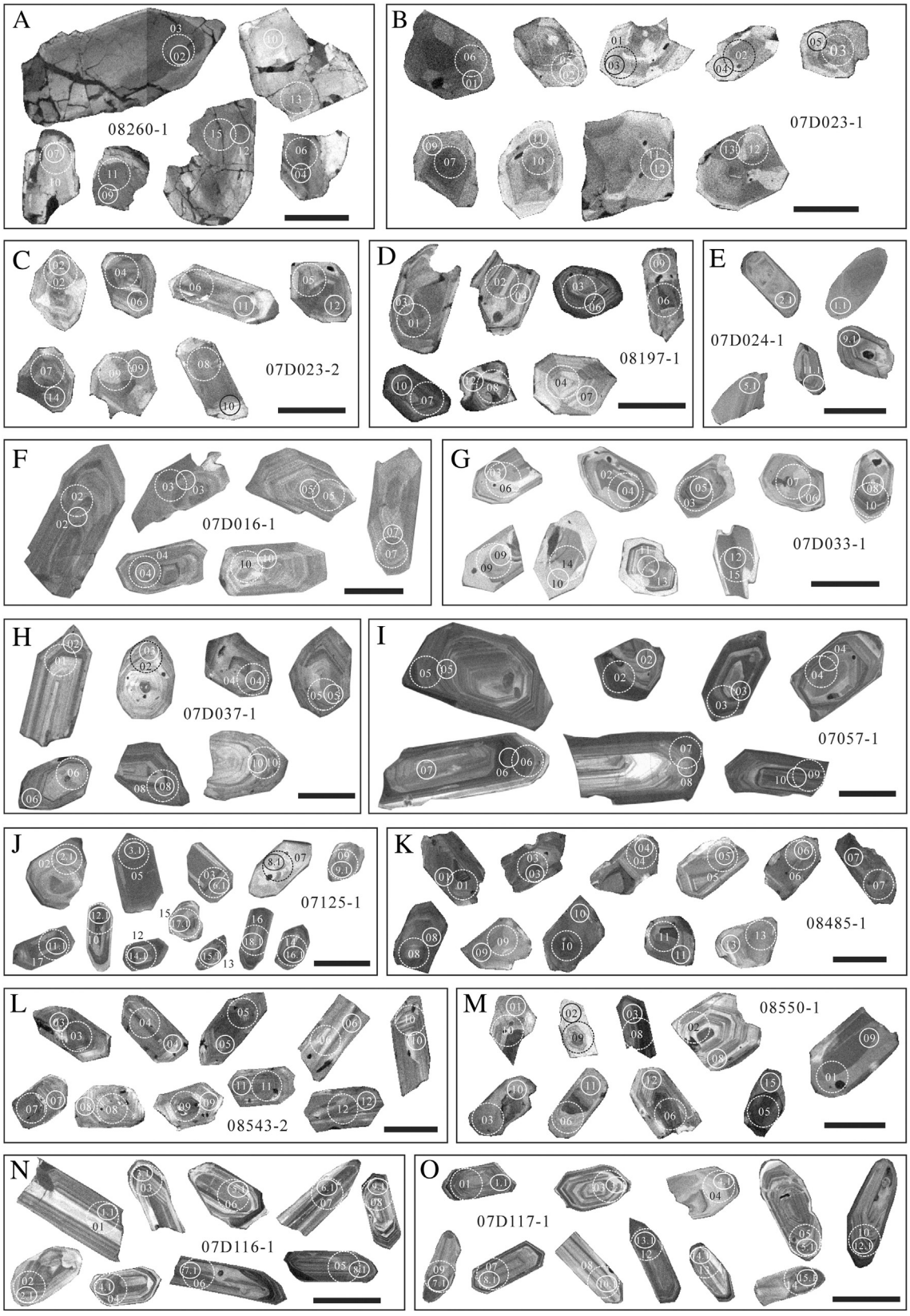

Fig. 5. Representative CL images, with SHRIMP and LA–ICP–MS U–Pb and in-situ Lu–Hf analyses spots of zircon grains. Small circles in (A)–(D), (F)–(I) and (K)–(M) are LA–ICP–MS U–Pb analysis spots. Ellipses in (E), (J), (N) and (O) are SHRIMP analysis spots. Large dashed circles are in-situ Lu–Hf analysis spots. Scale bar in each diagram is 100 μm long.

basalt, basalt, andesite, rhyodacite, dacite, trachyandesite and rhyolite. There is no significant gap between the mafic and felsic volcanic rocks in major and trace element classification diagrams (Fig. 7), which is very different from the chemical compositions of the bimodal volcanic rocks (e.g., Boardman and Condie, 1986; Ersoy et al., 2008; Mtoro et al., 2009).

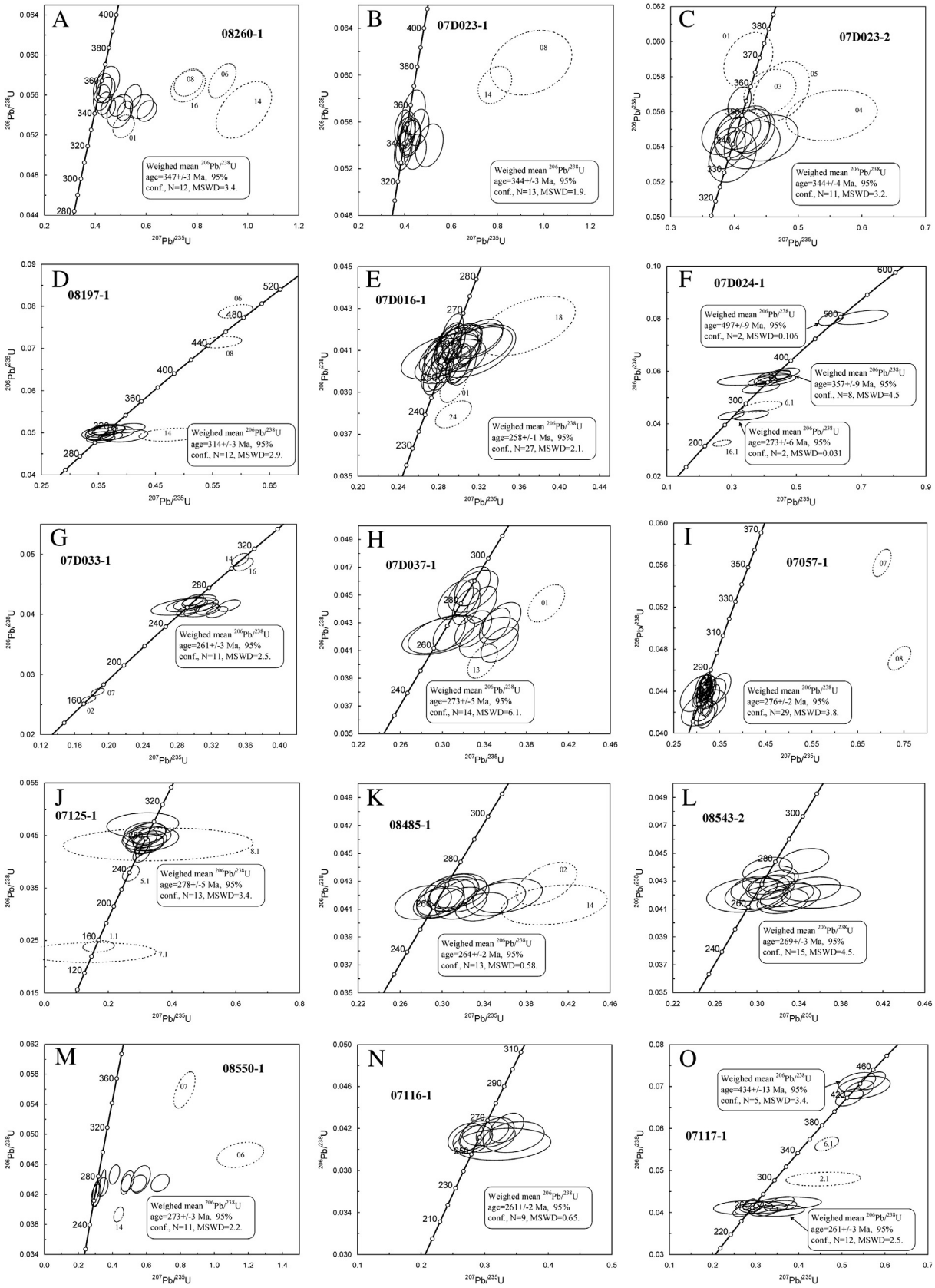

Fig. 6. U–Pb concordia diagrams for zircons from the Carboniferous–Permian volcanic rocks in the northern margin of the NCB. Data-point error crosses are 2σ.

The Carboniferous–Permian volcanic rocks in the northern margin of the NCB display total rare earth element (REE) contents from 56.0 to 420.1 ppm. Their chondrite-normalized REE patterns are shown in Fig. 8. Most samples exhibit similar REE patterns characterized by slight to significant LREE-enrichment (La_N/Yb_N = 3.02–25.54), no to weak negative Eu anomaly (Eu_N/Eu_N^* = 0.56–1.05) and flat heavy REE

Table 1
Summary of zircon U–Pb ages of the Carboniferous–Permian volcanic rocks in the northern margin of the NCB.

Sample no.	Latitude	Longitude	Location	Rock type	Age (Ma)	Method	References
99YG25	40°38′	110°22′	Yangkeleng	Volcanic ash	290 ± 6	SHRIMP	(Cope et al., 2005)
T3S-1	39°56′57″	115°55′30″	Western Beijing	Volcanic tuff	296 ± 4	SHRIMP	(Zhang et al., 2007b)
08260-1	42°00.85′	119°01.24′	Chifeng–Aohan	Andesitic basalt	347 ± 3	LA–ICP–MS	(This study)
07D023-1	42°24.16′	119°41.76′	Chifeng–Aohan	Brecciated rhyolite	344 ± 3	LA–ICP–MS	(This study)
07D023-2	42°24.16′	119°41.76′	Chifeng–Aohan	Brecciated dacite	344 ± 4	LA–ICP–MS	(This study)
08197-1	43°17.92′	118°38.18′	Chifeng–Aohan	Rhyolitic tuffaceous schist	314 ± 3	LA–ICP–MS	(This study)
07D016-1	42°30.54′	119°48.62′	Chifeng–Aohan	Dacite	258 ± 1	LA–ICP–MS	(This study)
07D024-1	42°24.40′	119°41.58′	Chifeng–Aohan	Andesite	273 ± 6	SHRIMP	(This study)
07D033-1	42°33.43′	118°57.08′	Chifeng–Aohan	Dacitic tuffaceous schist	261 ± 3	LA–ICP–MS	(This study)
07D037-1	42°37.76′	118°38.77′	Chifeng–Aohan	Rhyolitic tuff	273 ± 5	LA–ICP–MS	(This study)
07057-1	41°50.62′	112°51.18′	Sanjingquan	Rhyolitic tuff	276 ± 2	LA–ICP–MS	(This study)
07125-1	41°46.11′	110°32.64′	Damaoqi–Bayan Obo	Basaltic andesite	278 ± 5	SHRIMP	(This study)
08485-1	41°59.33′	111°34.24′	Damaoqi-Bayan Obo	Rhyolite	264 ± 2	LA–ICP–MS	(This study)
08543-2	41°50.61′	110°07.99′	Damaoqi–Bayan Obo	Rhyolite	269 ± 3	LA–ICP–MS	(This study)
08550-1	41°52.96′	109°59.24′	Damaoqi–Bayan Obo	Andesite	273 ± 3	LA–ICP–MS	(This study)
07116-1	41°56.73′	110°45.99′	Damaoqi–Bayan Obo	Rhyolitic porphyry	261 ± 2	SHRIMP	(This study)
07117-1	41°56.93′	110°45.36′	Damaoqi–Bayan Obo	Rhyolitic porphyry	261 ± 3	SHRIMP	(This study)

patterns. Several rhyolite and rhyolitic tuff samples (07D041-1, 08358-1, 07057-1, 07058-1, 08549-1) exhibit significant negative Eu anomaly ($Eu_N/Eu_N^* = 0.08–0.29$, Fig. 8E–G, I).

The trace element compositions of the basaltic samples are characterized by high contents of V (40.3–251.2 ppm), Cr (20.6–125.6 ppm), Co (26.4–40.36 ppm), Ni (26.4–39.7 ppm), Sr (665.6–1820.7 ppm), Ba (103.1–936.0 ppm), low content of Rb (1.4–52.3 ppm), and low Rb/Sr ratios (0.002–0.042). On primitive mantle-normalized diagrams (Fig. 9D), they display depletion in Rb, Nb, Ta, P, Zr, Hf, and Ti and enrichment in Ba, K and Sr. For the andesitic and dacitic rocks, they exhibit depletion in Nb, Ta, P, and Ti and enrichment in Th, U and K on primitive mantle-normalized diagrams (Fig. 9A–C, F, H). The rhyolitic rocks are characterized by low contents of V (1.9–38.8 ppm), Cr (0.13–26.1 ppm), Co (0.15–5.6 ppm), Ni (0.26–21.6 ppm), Rb (67.4–230.0 ppm), Ba (25.7–1453.0 ppm) and high Rb/Sr ratios (0.167–16.7). On primitive mantle-normalized diagrams (Fig. 9A, B, E–G, I, J), they display depletion in Nb, Ta, Sr, P, and Ti and enrichment in Rb, Th, U and K. In most cases, there is no depletion in Zr and Hf on primitive mantle-normalized diagrams of andesitic, dacitic and rhyolitic rocks (Fig. 9A–C, E–J).

4.3. Sr and Nd isotopic data

Whole-rock Sr–Nd isotopic data of the Carboniferous–Permian volcanic rocks in the northern margin of the NCB are listed in Table 2 and are plotted in Fig. 10. The volcanic rocks from northwestern Aohan (samples 07D023-1, 07D023-2, 07D016-1, 07D024-1, 07D025-1) are characterized by similar Sr–Nd isotopic compositions with low initial $^{87}Sr/^{86}Sr$ ratios of 0.70448–0.70694, high negative to near-zero $\varepsilon_{Nd}(t)$ values from −1.3 to 0.7 and Mesoproterozoic Nd isotopic T_{DM} model ages of 1.29–1.04 Ga. Those from northern and northwestern Chifeng (samples 07D028-1, 07D037-1) exhibit low initial $^{87}Sr/^{86}Sr$ ratios of 0.70347–0.70517, low negative $\varepsilon_{Nd}(t)$ values from −9.9 to −9.6 and old Nd isotopic T_{DM} model ages of 1.67–1.54 Ga. The basaltic andesite (sample 08359-2) from Xianghuangqi is characterized by high initial $^{87}Sr/^{86}Sr$ ratio of 0.70914, low negative $\varepsilon_{Nd}(t)$ value of −10.4 and old Nd isotopic T_{DM} model age of 1.87 Ga. However, rhyolite (sample 08358-1) exhibits high negative $\varepsilon_{Nd}(t)$ value of −3.9 and extremely low initial $^{87}Sr/^{86}Sr$ ratio of 0.69778, probably due to its high $^{87}Rb/^{86}Sr$ ratio (15.67). The volcanic rock from Sanjingquan (sample 07057-1) exhibits high initial $^{87}Sr/^{86}Sr$ ratio of 0.71550, low negative $\varepsilon_{Nd}(t)$ value of −12.1 and old Nd isotopic T_{DM} model age of 2.15 Ga. The basaltic andesite (sample 07125-1) from Damaoqi is characterized by low initial $^{87}Sr/^{86}Sr$ ratio of 0.70689, low negative $\varepsilon_{Nd}(t)$ value of −4.3 and Nd isotopic T_{DM} model age of 1.60 Ga. However, other volcanic rocks from Damaoqi-Bayan Obo area exhibit high initial $^{87}Sr/^{86}Sr$ ratios of 0.70948–0.71012, low negative $\varepsilon_{Nd}(t)$ values from −12.2 to −8.3 and Nd isotopic T_{DM} model ages of 1.99–1.59 Ga.

4.4. Lu–Hf isotopes of zircons

Zircon Lu–Hf isotopic data of the Carboniferous–Permian volcanic rocks in the northern margin of the NCB are listed in Supplementary Table A4 in the ESM and are plotted in Fig. 11. Zircons from the Early Carboniferous andesitic basalt (sample 08260-1) near Louzidian south to Chifeng are characterized by high initial $^{176}Hf/^{177}Hf$ ratios from 0.282463 to 0.282657, high negative to low positive $\varepsilon_{Hf}(t)$ values from −3.4 to 3.5, Hf isotopic T_{DM} model ages from 1.11 Ga to 0.84 Ga, and T_{DM}^C (crustal model ages) from 1.57 Ga to 1.13 Ga. Zircons from the Early Carboniferous brecciated rhyolite (sample 07D023-1) and brecciated dacite (07D023-2) in northwestern Aohan exhibit high initial $^{176}Hf/^{177}Hf$ ratios from 0.282481 to 0.282816, high negative to positive $\varepsilon_{Hf}(t)$ values from −2.7 to 9.1, Hf isotopic T_{DM} model ages from 1.11 Ga to 0.63 Ga, and T_{DM}^C from 1.53 Ga to 0.77 Ga. Synmagmatic zircons from the rhyolitic tuffaceous schist near the Xar Moron River north to Chifeng exhibit high initial $^{176}Hf/^{177}Hf$ ratios from 0.282505 to 0.282633, high negative to low positive $\varepsilon_{Hf}(t)$ values from −2.7 to 2.1, Hf isotopic T_{DM} model ages from 1.14 Ga to 0.90 Ga, and T_{DM}^C from 1.49 Ga to 1.20 Ga. Most zircons from the Late Permian dacite from the upper part of the volcanic sequences near Halagou northwest to Aohan are characterized by high initial $^{176}Hf/^{177}Hf$ ratios from 0.282623 to 0.282729, low positive $\varepsilon_{Hf}(t)$ values from 0.4 to 4.1, young Hf isotopic T_{DM} model ages from 0.89 Ga to 0.74 Ga, and T_{DM}^C from 1.26 Ga to 1.02 Ga. Synmagmatic zircons from the dacitic tuffaceous schist (sample 07D033-1) collected near Xiaowudetu north to Chifeng exhibit a wide range of Hf isotopic compositions with low initial $^{176}Hf/^{177}Hf$ ratios from 0.282091 to 0.282547, low and high negative $\varepsilon_{Hf}(t)$ values from −18.4 to −2.2, old Hf isotopic T_{DM} model ages from 1.66 Ga to 1.04 Ga, and T_{DM}^C from 2.44 Ga to 1.43 Ga. Zircons from the rhyolitic tuff (sample 07D037-1) near Dingjiawopu northwest to Chifeng low initial $^{176}Hf/^{177}Hf$ ratios from 0.282059 to 0.282226, low negative $\varepsilon_{Hf}(t)$ values from −19.0 to −13.1, old Hf isotopic T_{DM} model ages from 1.72 Ga to 1.44 Ga, and T_{DM}^C from 2.49 Ga to 2.13 Ga.

For the Early Permian rhyolitic tuff (sample 07057-1) collected from the volcanic sequence in Sanjingquan, northeast Siziwangqi, its zircons are characterized by similar zircon Hf isotopic compositions with low initial $^{176}Hf/^{177}Hf$ ratios from 0.282161 to 0.282257, low negative $\varepsilon_{Hf}(t)$ values from −15.4 to −12.1, old Hf isotopic T_{DM} model ages from 1.54 Ga to 1.40 Ga, and T_{DM}^C from 2.27 Ga to 2.06 Ga.

Synmagmatic zircons from the basaltic andesite (sample 07125-1) near Huxiye northeast to Damaoqi are characterized by variable Hf isotopic compositions with low initial $^{176}Hf/^{177}Hf$ ratios from 0.282141 to 0.282458, low negative $\varepsilon_{Hf}(t)$ values from −16.2 to −4.9, old Hf

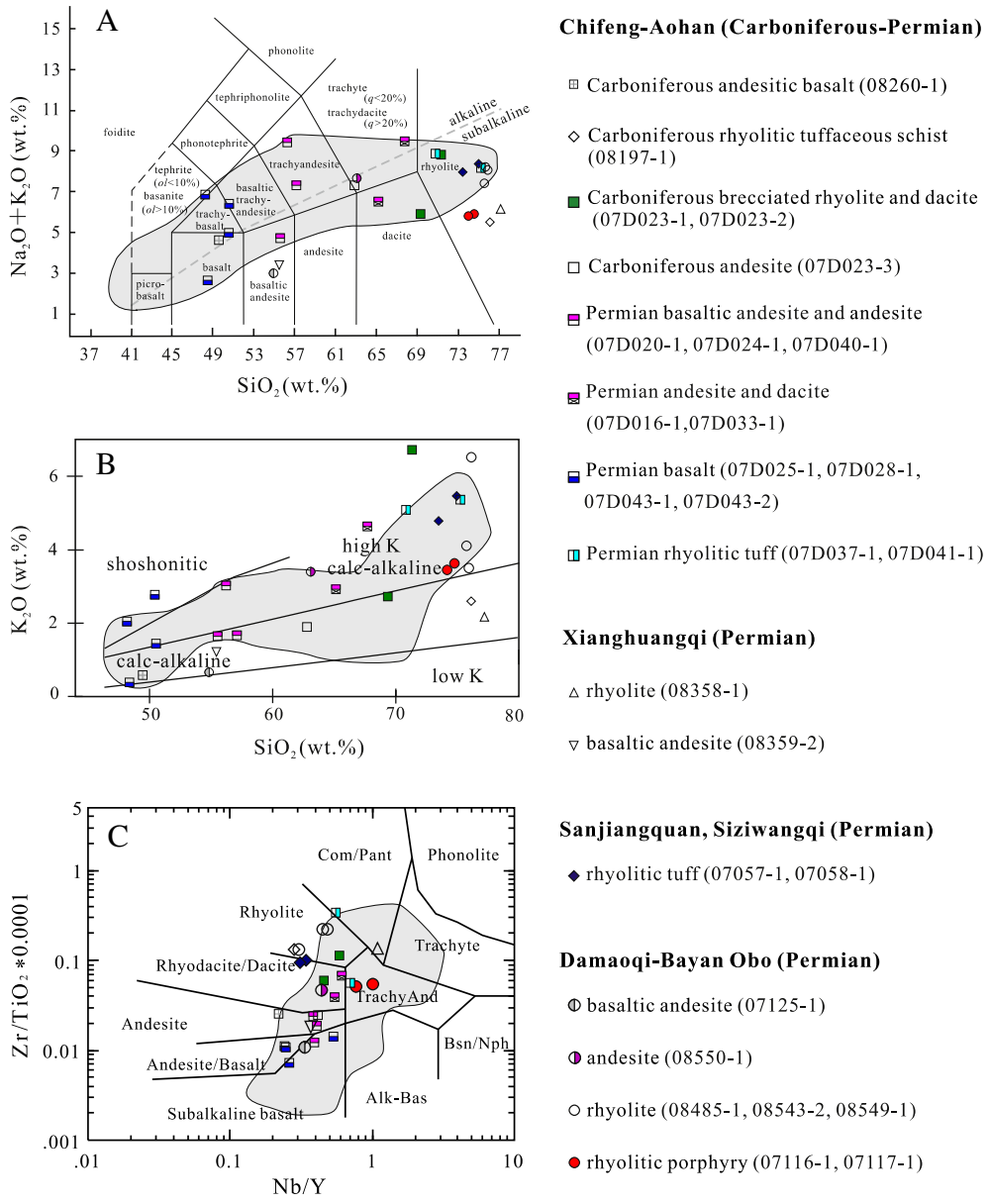

Fig. 7. (A) Total alkali (K_2O+Na_2O) vs. silica (SiO_2), (B) K_2O vs. SiO_2 and (C) Nb/Y vs. Zr/TiO_2 classification diagrams for the Carboniferous–Permian volcanic rocks in the northern NCB. Shaded areas show chemical compositions of the Carboniferous–Permian intrusive rocks in the northern margin of the NCC (Feng et al., 2009; Luo et al., 2009; Ma et al., 2013; Wang et al., 2009; Zhang et al., 2007a, 2009a,b,c, 2011a, 2012; Zhou et al., 2009).

isotopic T_{DM} model ages from 1.61 Ga to 1.10 Ga, and T_{DM}^{C} from 2.32 Ga to 1.62 Ga. Zircons from the rhyolite (samples 08485-1) near Baiyanhua northeast to Damaoqi exhibit high initial $^{176}Hf/^{177}Hf$ ratios from 0.282548 to 0.282958, high negative to positive $\varepsilon_{Hf}(t)$ values from −2.2 to 12.4, young Hf isotopic T_{DM} model ages from 1.01 Ga to 0.42 Ga, and T_{DM}^{C} from 1.43 Ga to 0.50 Ga. Zircons from the rhyolite (samples 08543-2) near Bayinaobao Sum northwest to Damaoqi exhibit low initial $^{176}Hf/^{177}Hf$ ratios from 0.282285 to 0.282506, negative $\varepsilon_{Hf}(t)$ values from −11.3 to −3.5, old Hf isotopic T_{DM} model ages from 1.40 Ga to 1.08 Ga, and T_{DM}^{C} from 2.01 Ga to 1.52 Ga. Synmagmatic zircons from the andesite (sample 08550-1) near Agui northeast to Bayan Obo are characterized by low initial $^{176}Hf/^{177}Hf$ ratios from 0.281807 to 0.282374, low negative $\varepsilon_{Hf}(t)$ values from −28.0 to −8.0, old Hf isotopic T_{DM} model ages from 2.01 Ga to 1.25 Ga, and T_{DM}^{C} from 3.05 Ga to 1.81 Ga. Synmagmatic zircons from the rhyolitic porphyry samples (07116-1 and 07117-1) near Chaganaobao Sumu northeast to Damaoqi exhibit low initial $^{176}Hf/^{177}Hf$ ratios from 0.282358 to 0.282596, high negative $\varepsilon_{Hf}(t)$ values from −8.9 to −0.6, Hf isotopic T_{DM} model ages from 1.30 Ga to 0.95 Ga, and T_{DM}^{C} from 1.85 Ga to 1.32 Ga.

5. Discussion

5.1. Eruption ages of the Carboniferous–Permian volcanic rocks in the northern margin of the NCB

As shown in Table 1, our new results show that eruption of the Carboniferous–Permian volcanic rocks in the northern margin of the NCB occurred during the Early Carboniferous to Late Permian from 347 ± 3 Ma to 258 ± 1 Ma. The new zircon U–Pb results of volcanic rocks provide important constraints on correlation of the Late Paleozoic strata in the northern NCB as well as temporal and spatial variations of the Carboniferous–Permian volcanic rocks (Fig. 2).

The Carboniferous–Permian volcanic rocks are well outcropped in Chifeng–Aohan area in the eastern part of the northern margin of the NCB with zircon U–Pb ages from 347 ± 3 Ma to 258 ± 1 Ma. It seems

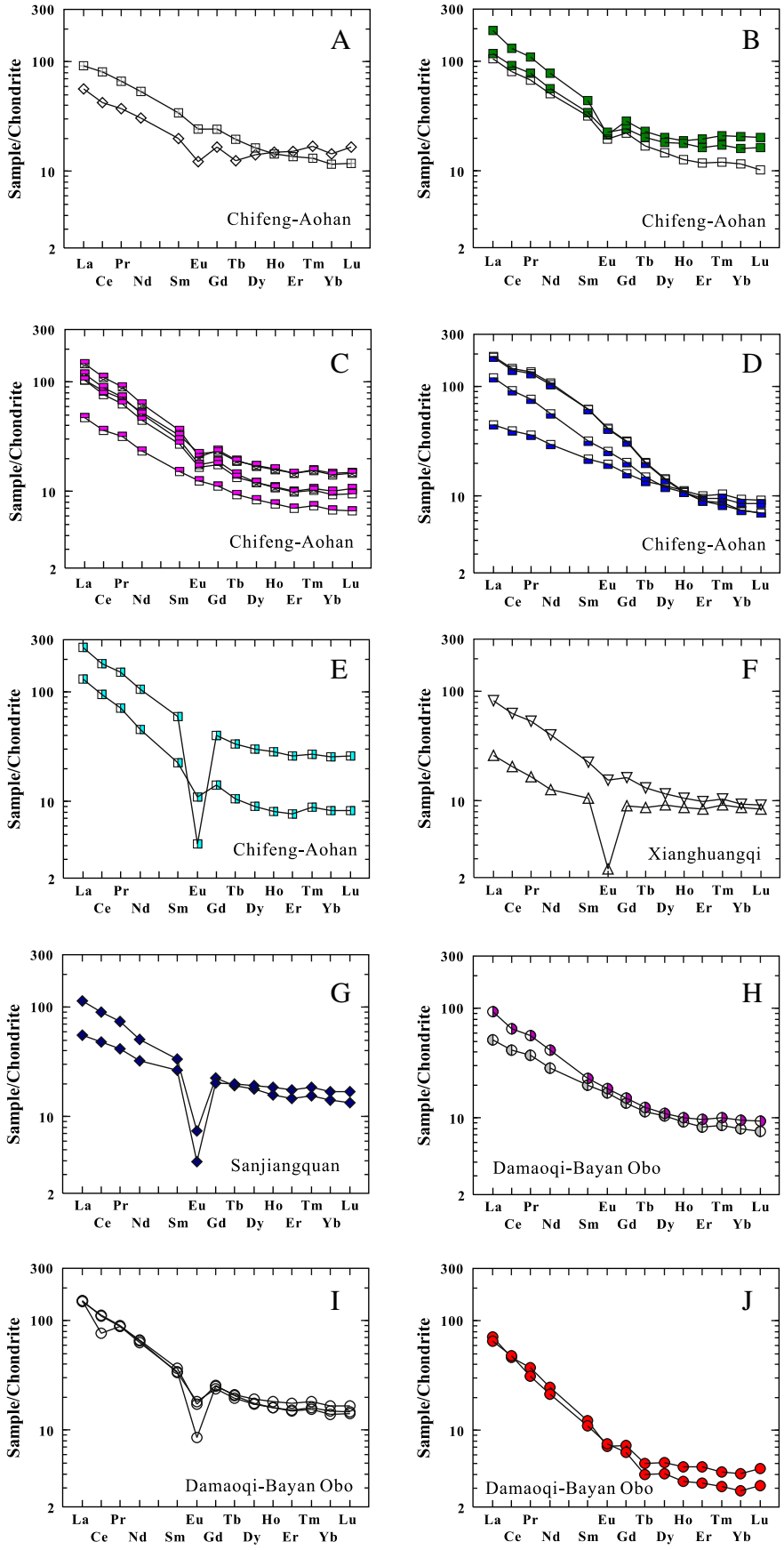

Fig. 8. Chondrite-normalized REE patterns for the Carboniferous–Permian volcanic rocks in the northern NCB. The chondrite values are from Taylor and McLennan (1985). Symbols are same as Fig. 7.

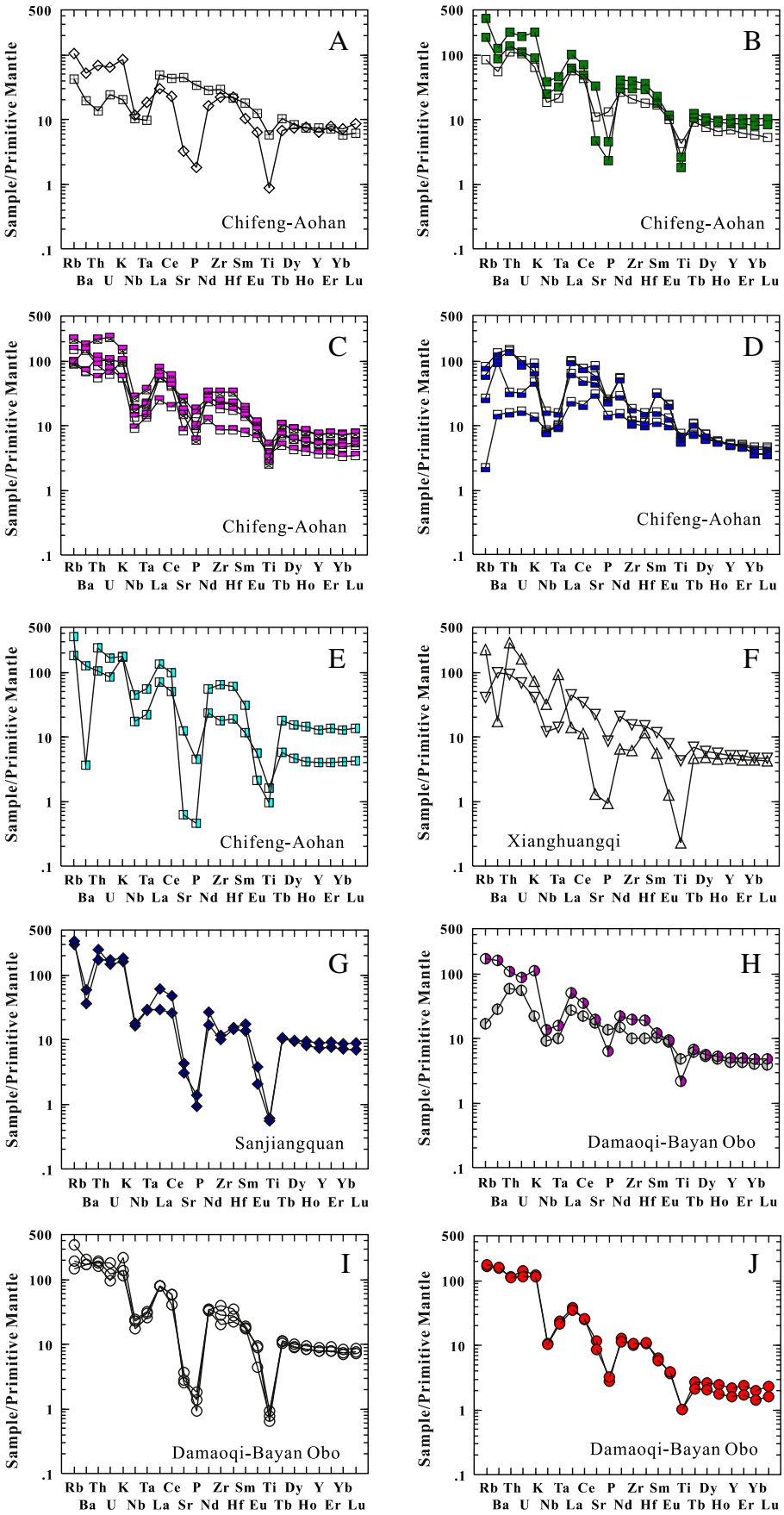

Fig. 9. Primitive mantle-normalized spidergrams for the Carboniferous–Permian volcanic rocks in the northern NCB. The primitive mantle values are from Sun and McDonough (1989). Symbols are same as Fig. 7.

Table 2
Rb–Sr and Sm–Nd isotopes of the Carboniferous–Permian volcanic rocks in the northern margin of the NCB.

Sample no.	Age (Ma)	SiO_2 (wt.%)	Mg#	Rb	Sr	$^{87}Rb/^{86}Sr$	$^{87}Sr/^{86}Sr$ (2σ)	$(^{87}Sr/^{86}Sr)_i$	Sm	Nd	$^{147}Sm/^{144}Nd$	$^{143}Nd/^{144}Nd$ (2σ)	$(^{143}Nd/^{144}Nd)_i$	$\varepsilon_{Nd}(0)$	$\varepsilon_{Nd}(t)$	$f_{Sm/Nd}$	T_{DM}
Chifeng–Aohan																	
07D023-1	344	71.3	26.39	198.0	93.0	6.1687	0.734683 ± 12	0.704481	10.0	56.6	0.1072	0.512369 ± 5	0.512128	−5.3	−1.3	−0.46	1117
07D023-2	344	69.3	51.59	119.2	736.2	0.4687	0.709237 ± 14	0.706942	7.89	39.79	0.1200	0.512406 ± 13	0.512136	−4.5	−1.2	−0.39	1210
07D016-1	258	67.7	33.17	140.8	311.2	1.3095	0.710377 ± 14	0.705571	7.89	42.55	0.1123	0.512458 ± 12	0.512268	−3.5	−0.7	−0.43	1040
07D024-1	270	55.5	62.06	56.2	558.0	0.2914	0.707223 ± 13	0.706104	4.09	18.77	0.1318	0.512472 ± 12	0.512239	−3.2	−1.0	−0.33	1260
07D025-1	270	48.4	51.28	2.1	656.4	0.0091	0.706687 ± 12	0.706652	6.27	25.77	0.1474	0.512589 ± 12	0.512328	−1.0	0.7	−0.25	1289
07D028-1	270	50.5	49.26	16.5	965.0	0.0494	0.703662 ± 13	0.703472	7.38	41.37	0.1080	0.511990 ± 12	0.511799	−12.6	−9.6	−0.45	1668
07D037-1	273	70.8	38.80	118.4	266.4	1.2871	0.710168 ± 12	0.705169	4.98	31.66	0.0952	0.511950 ± 17	0.511780	−13.4	−9.9	−0.52	1541
Xianghuangqi																	
08358-1	270	77.1	24.35	143.5	26.7	15.6650	0.757950 ± 12	0.697775	2.55	8.69	0.1779	0.512405 ± 15	0.512090	−4.6	−3.9	−0.10	3149
08359-2	270	55.5	52.97	24.7	463.5	0.1544	0.709734 ± 15	0.709141	5.16	26.64	0.1173	0.511964 ± 15	0.511757	−13.2	−10.4	−0.40	1870
Sanjingquan																	
07057-1	276	73.5	21.83	219.1	87.3	7.2892	0.744128 ± 10	0.715504	7.99	38.83	0.1245	0.511885 ± 14	0.511660	−14.7	−12.1	−0.37	2153
Damaoqi–Bayan Obo																	
07125-1	278	54.9	50.94	11.8	379.6	0.0897	0.707248 ± 13	0.706894	4.80	21.93	0.1326	0.512299 ± 13	0.512058	−6.6	−4.3	−0.33	1596
08485-1	264	75.9	15.66	227.7	82.9	7.9768	0.740079 ± 15	0.710119	9.10	48.41	0.1138	0.512068 ± 13	0.511871	−11.1	−8.3	−0.42	1648
08543-2	269	75.7	7.39	93.5	53.8	5.0362	0.728791 ± 13	0.709517	9.14	52.34	0.1057	0.512018 ± 15	0.511832	−12.1	−9.0	−0.46	1593
08550-1	273	63.0	34.60	95.3	429.5	0.6424	0.711981 ± 13	0.709486	5.21	27.24	0.1158	0.511870 ± 23	0.511663	−15.0	−12.2	−0.41	1987

$f_{Sm/Nd} = (^{147}Sm/^{144}Nd)_{sample}/(^{147}Sm/^{144}Nd)_{CHUR}-1$; $T_{DM} = 1/\lambda\times\ln\{1+[(^{143}Nd/^{144}Nd)_{sample} - (^{143}Nd/^{144}Nd)_{DM}]/[(^{147}Sm/^{144}Nd)_{sample} - (^{147}Sm/^{144}Nd)_{DM}]\}$. The $^{143}Nd/^{144}Nd$ and $^{147}Sm/^{144}Nd$ ratios of chondrite and depleted mantle at present day are 0.512638 and 0.1967, 0.51315 and 0.2137, respectively.

there is a northward younging trend of the volcanic rocks in Chifeng–Aohan area (Figs. 1B and 2E–G), which is likely related to rollback of the subducted Paleo-Asian oceanic plate. Although some Carboniferous dioritic intrusions have been reported from the middle-western part of the Inner Mongolia Paleo-uplift (e.g., Liu et al., 2014; Zhang et al., 2012; Zhou et al., 2009), no Carboniferous volcanic rocks have been identified from the middle-western parts of the northern margin of the NCB. Our geochronological results of the volcanic rocks from Sanjiangquan and Bayan Obo–Damaoqi areas indicate that the eruption of the volcanic rocks in the middle-western parts of the northern margin of the NCB occurred during the Early–Middle Permian from 278 ± 5 Ma to 261 ± 3 Ma. From the Carboniferous to Permian, the proportions of rhyolite and rhyolitic tuff in the volcanic sequences were increasing. As shown in Fig. 2, the upper limits of the Carboniferous–Permian volcanic sequences in the northern margin of the NCB tend to decrease slightly from west to east, suggesting that decease of subduction of the Paleo-Asian oceanic plate beneath the northern NCB in the middle-western parts is a little earlier than that in the eastern part.

5.2. Petrogenesis and tectonic setting of the volcanic rocks

As shown above, the Carboniferous–Permian volcanic rocks in the northern NCB are characterized by variable SiO_2 contents from 48.2 wt.% to 77.1 wt.% and a rock association of basalt, basaltic andesite, andesite, dacite, rhyolite, tuff, tufaceous sandstone and minor hypabyssal rocks such as rhyolitic porphyry. This rock association is very similar to that of the continental arc magmatism (e.g., Murphy, 2006; Wilson, 1989). Formation of the Carboniferous–Permian volcanic rocks in arc tectonic setting is further confirmed by negative Nb and Ta anomalies of mafic to intermediate rocks on primitive mantle-normalized diagrams (Fig. 9A–D, H), which is a characteristic feature shared by many subduction-related magmatic rocks (e.g., Briqueu et al., 1984; Murphy, 2007; Rogers and Hawkesworth, 1989).

Although the Carboniferous–Permian volcanic rocks were formed in an Andean-type continental margin and were related to southward subduction of the Paleo-Asian oceanic plate beneath the northern NCB, their variable SiO_2 contents and wide ranges of whole-rock Sr–Nd and zircon Hf isotopic compositions (Table 2 and Supplementary Table A4 in the ESM, Figs. 10 and 11) indicate that their source areas are very complex. Similar to the Carboniferous intrusions consisting mainly of gabbro, gabbroic diorite, diorite and tonalite (Fig. 7), the Early Carboniferous volcanic rocks from Chifeng–Aohan area are composed mainly of basalt, basaltic andesite, andesite and minor dacite and rhyolite (Fig. 2E–G). They are characterized by variable SiO_2 contents from 49.5 wt.% to 71.3 wt.% and Mg# values of 26.4–51.6. They exhibit low initial $^{87}Sr/^{86}Sr$ ratios of 0.70448–0.70694, high negative to positive $\varepsilon_{Nd}(t)$ and $\varepsilon_{Hf}(t)$ values, and relatively young Nd and Hf isotopic model ages. These geochemical characteristics indicate that the Early Carboniferous volcanic rocks were likely produced by fractional crystallization of mafic magma derived from partial melting of the mantle wedge and subducted oceanic crust of the Paleo-Asian ocean.

The Permian volcanic rocks consist mainly of basalt, basaltic andesite, andesite, dacite, rhyolite, tuff and tuffaceous sandstone. Compared with the Carboniferous volcanic rocks, rhyolite and rhyolitic tuff are more common in the Permian volcanic sequences, indicating more involvement of crustal materials in formation of the Permian volcanic rocks. The Permian basalts and basaltic andesites are characterized by low content of SiO_2 (48.2–55.5 wt.%), high contents of V (40.3–251.2 ppm), Cr (20.6–352.9 ppm), Co (23.5–40.3 ppm), Ni (26.4–109.2 ppm), Fe_2O_3T (7.3–12.1 wt.%), CaO (7.4–10.2 wt.%) and MgO (4.5–6.4 wt.%), and high Mg# values of 49.3–62.1. They exhibit low initial $^{87}Sr/^{86}Sr$ ratios of 0.70347–0.70914, negative to low positive $\varepsilon_{Nd}(t)$ values from −10.4 to 0.7 and Nd isotopic T_{DM} model ages of 1.87–1.26 Ga, and negative $\varepsilon_{Hf}(t)$ values from −16.2 to −4.9, old Hf isotopic T_{DM} model ages from 1.61 Ga to 1.10 Ga, and T^{C}_{DM} from 2.32 Ga to 1.62 Ga. These geochemical characteristics suggest that the Permian

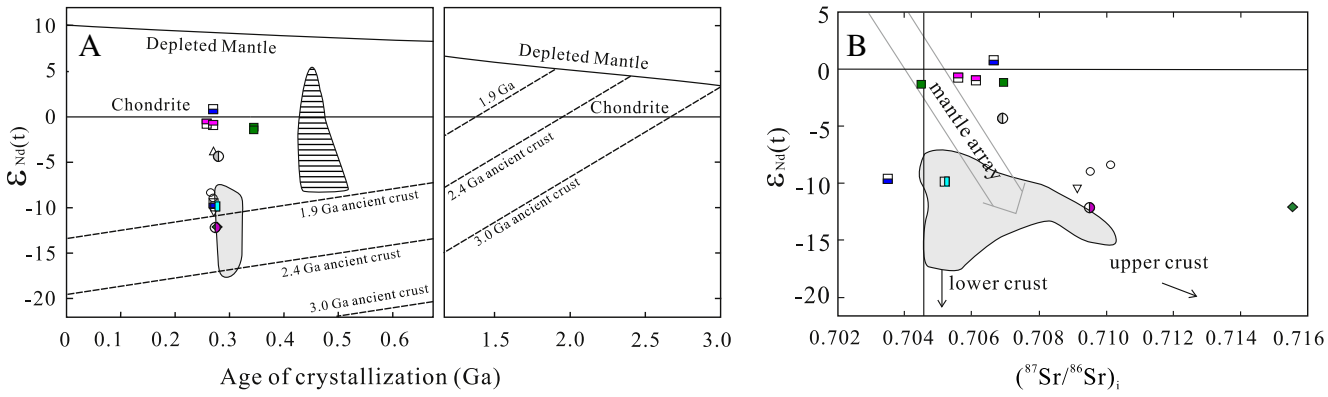

Fig. 10. (A) $\varepsilon_{Nd}(T)$ vs. crystallization age and (B) $\varepsilon_{Nd}(T)$ vs. $(^{87}Sr/^{86}Sr)_i$ plots for the Carboniferous–Permian volcanic rocks. Area with horizontal lines in (A) shows Nd isotopic compositions of the Early Paleozoic magmatic rocks in the Bainaimiao arc belt (Zhang et al., 2014). Shaded areas in (A) and (B) show Sr–Nd isotopic compositions of the Carboniferous–Permian intrusive rocks in the northern margin of the NCC (Feng et al., 2009; Ma et al., 2013; Wang et al., 2009; Zhang et al., 2009a,b,c, 2011a, 2012). The ancient crust evolution line in (A) is constructed on the basis of an average $^{147}Sm/^{144}Nd$ value of 0.118 (Jahn and Condie, 1995). Symbols are same as Fig. 7.

basalts and basaltic andesites were produced by partial melting of a mantle wedge that was metasomatized by hydrous fluids derived from subducted oceanic crust. Assimilation of crustal materials may have occurred during magma ascent, as indicated by the relatively high initial $^{87}Sr/^{86}Sr$ ratios (0.70914), low positive $\varepsilon_{Nd}(t)$ values (−12.1) and old Nd isotopic T_{DM} model ages (1.87 Ga) of the basaltic andesite from Xianghuangqi (sample 08359-2).

Compared with basalt and basaltic andesite, the andesite, dacite, rhyolite and rhyolitic tuff are more common among Permian volcanic rocks, suggesting they are not produced by fractional crystallization of mafic magma gave rise to the Permian basalt and basaltic andesite. They exhibit high contents of SiO_2 (56.2–77.1 wt.%), low content of MgO (0.05–2.0 wt.%) and low Mg# values of 7.4–48.1, indicating they were mainly crust-derived, probably related to underplating of the mafic magma derived from partial melting of the mantle wedge and subducted oceanic crust. There is a striking correlation between the whole-rock Sr–Nd and zircon Hf isotopic compositions of the Permian andesite, dacite and rhyolitic volcanic rocks and those of the underlying basement. Those located in the NCC (samples 07D033-1, 07D037-1, 07057-1, 08543-2, 08550-1) are mainly characterized by low negative $\varepsilon_{Nd}(t)$ and $\varepsilon_{Hf}(t)$ values and old Nd and Hf isotopic model ages. In the $\varepsilon_{Nd}(T)$ vs. crystallization age and $\varepsilon_{Hf}(t)$ vs. zircon U–Pb age plots (Figs. 10A and 11), they mainly fall into the areas between or near the evolutionary trend lines for 1.9 Ga and 2.5 Ga ancient crust, indicating they are mainly produced by partial melting of the Paleoproterozoic ancient crust of the NCC. In contrast, those located in the Bainaimai arc belt or the Bayan Obo–Duolun–Chifeng–Kaiyuan fault zone (samples 07D016-1, 08358-1, 08485-1, 07116-1, 07117-1) exhibit relative high $\varepsilon_{Nd}(t)$ and $\varepsilon_{Hf}(t)$ values and young Nd and Hf isotopic model ages. In the $\varepsilon_{Nd}(T)$ vs. crystallization age and $\varepsilon_{Hf}(t)$ vs. zircon U–Pb age plots (Figs. 10A and 11), they mainly fall into an area far above the evolutionary trend lines for 1.9 Ga ancient crust. They were likely produced by partial melting of the lower arc continental crust of the Bainaimiao arc belt. As shown by our previous study (Zhang et al., 2014), the Bainaimiao arc belt is an ensialic island arc formed during the Early Cambrian to Middle Silurian (0.52–0.42 Ga) and was developed upon some crustal fragments with affinity to the Tarim or Yangtze (South China) cratons. The Sr–Nd–Hf isotopic differences between the Permian felsic volcanic rocks from either side of the Bayan Obo–Duolun–Chifeng–Kaiyuan fault zone (northern boundary fault of the NCC) further support that the basement compositions of the Bainaimiao arc belt are very different from those of the NCC as suggested by our previous study (Zhang et al., 2014).

5.3. Implications for generation of the continental arc volcanism and the MASH hypothesis

In contrast to volcanic rocks in oceanic island arcs dominated by mafic to intermediate magmas and generated mainly by partial melting of the mantle wedge and/or subducted oceanic crust, origin of the volcanic rocks in continental arcs is very complex due to their thick continental crust (e.g., Lee and Bachmann, 2014; Murphy, 2006; Wilson, 1989). As shown in many research results from continental arcs in western South and North America, materials from the subducted oceanic crust

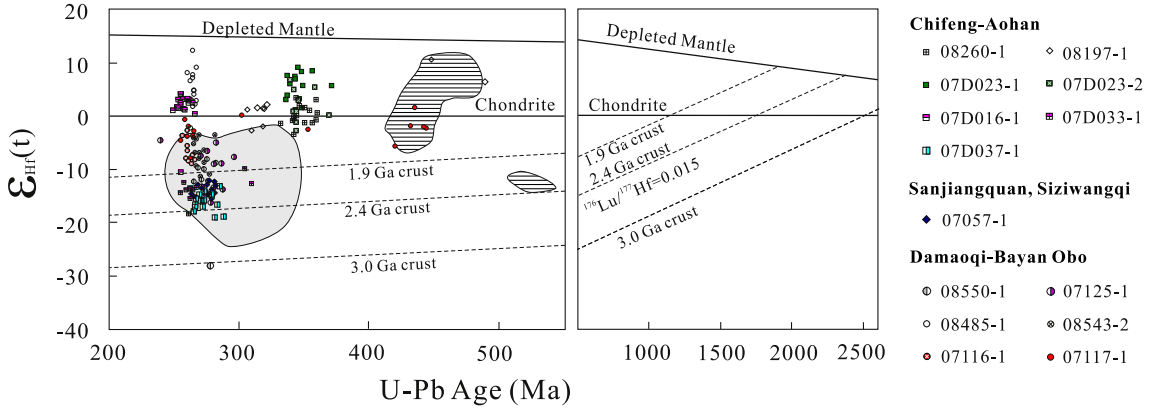

Fig. 11. $\varepsilon_{Hf}(t)$ vs. U–Pb age of zircons from the Carboniferous–Permian volcanic rocks. Areas with horizontal lines show Hf isotopic compositions of zircons from the Early Paleozoic magmatic rocks in the Bainaimiao arc belt (Zhang et al., 2014). Shaded area shows Hf isotopic compositions of zircons from the Carboniferous–Permian intrusive rocks in the northern margin of the NCC (Bai et al., 2013; Feng et al., 2009; Ma et al., 2013; Wang et al., 2009; Zhang et al., 2009a,b,c, 2011a, 2012).

and sediments, mantle wedge and arc continental crust could be involved in the generation of arc magmatism and their source areas could be temporally and spatially different (e.g., Feeley et al., 1998; Gómez-Tuena et al., 2003, 2007, 2014; Haschke et al., 2006; Hildreth and Moorbath, 1988; Kay et al., 2005; Lucassen et al., 2006; Mamani et al., 2010; McMillan et al., 1989; Murphy, 2007; Ramos, 1999; Stern and Kilian, 1996). In the Central Volcanic Zone of Andean Arc, there is a striking correlation between the isotopic compositions of the volcanic rocks and those of the underlying basement (e.g., Wörner et al., 1994). Although the basalt, andesitic basalt and some andesite in the northern NCB were produced by fractional crystallization of mafic magma derived from partial melting of mantle wedge and subducted oceanic crust of the Paleo-Asian ocean, most of the intermediate to felsic volcanic rocks were derived from partial melting of lower continental crust. Similar to the arc volcanism in the Central Volcanic Zone of Andean Arc, there is a striking correlation between the whole-rock Sr–Nd and zircon Hf isotopic compositions of the Permian intermediate to felsic volcanic rocks and those of the underlying basement, further indicating crustal origin for the Permian intermediate to felsic arc volcanic rocks in the northern NCB. From the Carboniferous to Permian, involvement of crustal materials increased significantly, as suggested by increasing volumes of felsic volcanic rocks in the Carboniferous–Permian volcanic sequences. Our results on the Carboniferous–Permian volcanic rocks in the northern NCB further indicate that origin of continental arc volcanism is very complex and both materials from the subducted oceanic crust and sediments, mantle wedge and arc continental crust could be involved in the generation of arc volcanic rocks.

Based on chemical and isotopic studies of arc magmatism in the Andes of Central Chile, a melting–assimilation–storage–homogenization (MASH) model was proposed by Hildreth and Moorbath (1988). The MASH model has been widely accepted by many researchers and is considered an important process for formation of intermediate to felsic magmatic rocks in continental arcs (e.g., Davidson et al., 1990; de Silva et al., 2015; Ducea et al., 2015; Folkes et al., 2011; Hart et al., 2002; Jicha et al., 2007; Kay and Gordillo, 1994; Kleine et al., 2004; Lackey et al., 2005; Lake and Farmer, 2015; Li et al., 2014; Matteini et al., 2002; Muñoz et al., 2012; Ort et al., 1996; Richards, 2003, 2005; Riley et al., 2001; Tassara, 2006; Zhang et al., 2009a,b). In the MASH zone usually located in the lowermost crust or mantle-crust transition, conditions are favorable for high-volume dehydration partial melting of preexisting ancient lower-crustal rocks to produce large volume of intermediate to felsic magmatic rocks (e.g., Lackey et al., 2005). However, the degree of homogenization in the MASH zone is still poorly understood (Ducea et al., 2015). Although magmas in the MASH zone within continental arcs could be mixed extensively to generate homogenized magmas (e.g., Folkes et al., 2011; Lackey et al., 2005), some results show that the above mixture and homogenization are likely incomplete (e.g., Ort et al., 1996).

Our previous results on the Carboniferous–Permian intrusive rocks from the northern margin of the NCC indicate that MASH processes occurred during formation of the arc magmatism (Zhang et al., 2009a,b). Although the Carboniferous–Permian granitoids in the northern margin of the NCC are characterized by similar Sr–Nd–Hf isotopic compositions with low negative $\varepsilon_{Nd}(t)$ and $\varepsilon_{Hf}(t)$ values and old Nd and Hf isotopic model ages (e.g., Bai et al., 2013; Luo et al., 2009; Ma et al., 2013; Zhang et al., 2009a,b, 2011a, 2012), there are significant differences between the isotopic compositions of magmatic rocks from either side of the Bayan Obo–Duolun–Chifeng–Kaiyuan fault zone. Since most of these intermediate to felsic magmatic rocks are mainly crustal-derived, their differences reflect the age and isotopic differences of the underlying basement from either side of the fault. The striking correlation between the whole-rock Sr–Nd and zircon Hf isotopic compositions of the Permian andesite, dacite and rhyolitic volcanic rocks and those of the underlying basement in the northern NCB revealed in this presentation indicates that magma homogenization and mixture in the MASH zones within the North China continental arc was most likely incomplete. The above inference is further supported by the striking correlation between the isotopic compositions of the volcanic rocks and those of the underlying basement in the Central Volcanic Zone of Andean Arc (e.g., Wörner et al., 1994). Therefore, incomplete homogenization of magmas is likely a common feature of many MASH zones in continental arcs. Considering the incomplete homogenization of magmas in many MASH zones within many continental arcs, it is much accurate to use mixing–assimilation–storage–hybridization or melting–assimilation–storage–hybridization for MASH processes as suggested by Annen et al. (2006) and Solano et al. (2012), respectively.

6. Conclusions

(1) The Carboniferous–Permian volcanic rocks in the northern NCB exhibit features of continental arc magmatism with variable SiO_2 contents (48.2–77.1 wt.%), calc-alkaline composition and a rock association of basalt, basaltic andesite, andesite, dacite, rhyolite, tuff, tufaceous sandstone and minor hypabyssal rocks. They exhibit subduction-related geochemical features and were formed in an Andean-type continental arc during southward subduction of the Paleo-Asian oceanic plate beneath the northern NCB.

(2) Eruption of the Carboniferous–Permian volcanic rocks in the northern margin of the NCB occurred during the Early Carboniferous to Late Permian from 347 ± 3 Ma to 258 ± 1 Ma. The upper limits of the Carboniferous–Permian volcanic sequences in the northern margin of the NCB tend to decrease slightly from west to east, suggesting that decease of subduction of the Paleo-Asian oceanic plate beneath the northern NCB in its middle-western parts is a little earlier than that in its eastern part.

(3) The Carboniferous–Permian volcanic rocks exhibit a wide range of whole-rock Sr–Nd and zircon Hf isotopic compositions, indicating that their source areas are very complex. The basalt, andesitic basalt and some andesite were produced by fractional crystallization of mafic magma derived from partial melting of mantle wedge and subducted oceanic crust of the Paleo-Asian ocean. However, most of the intermediate to felsic volcanic rocks were derived from partial melting of lower arc continental crust. There is an increasing input of crustal materials from the Carboniferous to Permian as indicated by increasing volume of felsic volcanic rocks in the volcanic sequences.

(4) Our results on the Carboniferous–Permian volcanic rocks in the northern NCB indicate that origin of the continental arc volcanism is very complex and both materials from the subducted oceanic crust and sediments, mantle wedge and arc continental crust could be involved in the generation of arc volcanic rocks.

(5) There is a striking correlation between the whole-rock Sr–Nd and zircon Hf isotopic compositions of the Permian andesite, dacite and rhyolitic volcanic rocks and those of the underlying basement. Sr–Nd–Hf isotopic differences between the Permian intermediate to felsic volcanic rocks from either side of the northern boundary fault of the NCC suggest that mixture and homogenization of the magmas in the MASH zone within this continental arc was incomplete, and incomplete homogenization of magmas is likely a common feature of many MASH zones in continental arcs.

Acknowledgments

This research was financially supported by the China Geological Survey (grants 1212010050504-3 and 1212010711817), the National Natural Science Foundation of China (41372230) and the International Science and Technology Cooperation Program of China (2014DFR 21270). We thank Y.S. Liu, X.M. Liu, C.F. Li, B. Song, C.Y. Diwu, Y.R. Shi,

W. Zhang, K.J. Hou, X.D. Jin and H. Li for their analytical assistance. Careful and constructive reviews by W.J. Xiao, A. Barth and G.N. Eby (Editor-in-Chief) significantly improved the quality of the manuscript.

Appendix A. Analytical methods

A.1. Sample preparation and imaging

Zircons were separated using conventional crushing and separation techniques and were then handpicked under a binocular microscope. They were mounted in epoxy resin together with the M257 and TEMORA zircon standards and polished to expose the cores of the grains in readiness for cathodoluminescence (CL), SHRIMP or LA–ICP–MS U–Pb and in-situ Lu–Hf isotopic analyses. Zircons were imaged using the HITACHI S3000-N electron microscope attached with a GATAN Chroma CL detector at the Beijing SHRIMP Center. CL images of representative zircon grains are shown in Fig. 5.

A.2. SHRIMP and LA–ICP–MS U–Pb analysis

SHRIMP U–Pb dating was performed on the SHRIMP II at the Beijing SHRIMP Center following the method of Williams (1998). The mass resolution was ca. 5000 at 1% peak height. The spot size of the ion beam was 25–30 μm, and five scans through the mass range were used for data collection. The M257 (561 Ma, U = 840 ppm, Nasdala et al., 2008) and TEMORA (417 Ma) standards (Black et al., 2003) were used in the analyses for U concentration and age calibration, respectively. Sites for dating were selected on the basis of CL and photomicrograph images. Ages and concordia diagrams were produced using the programs SQUID 1.03 (Ludwig, 2001) and ISOPLOT/Ex 3.23 (Ludwig, 2003).

LA–ICP–MS U–Pb and trace element analyses were performed on an excimer (193 nm wavelength) LA–ICP–MS at the State Key Laboratory of Geological Processes and Mineral Resources, China University of Geosciences, Wuhan and the State Key Laboratory of Continental Dynamics, Northwest University, Xi'an. Detailed operating conditions for the laser ablation system and the ICP–MS instrument and data reduction are the same as described by Liu et al. (2008, 2010a,b) and Yuan et al. (2004), respectively. The ICP–MS used is an Agilent 7500a. The GeoLas 2005 laser-ablation system was used for the laser ablation experiments. Nitrogen was added into the central gas flow (Ar+He) of the Ar plasma to decrease the detection limit and improve precision (Hu et al., 2008). Sites for analyses were selected on the basis of CL and photomicrograph images. The spots used were 30–32 μm in diameter. U, Th and Pb concentrations were calibrated by using ^{29}Si as an internal standard and NIST SRM 610 as the reference standard. Isotopic ratios were calculated using GLITTER 4.0 (Macquarie University) and ICPMSDataCal 5.0 (Liu et al., 2008, 2010a), which were then corrected for both instrumental mass bias and depth-dependent elemental and isotopic fractionation using Harvard zircon 91500 as external standard. GEMOC GJ-1 zircon standard (TIMS U–Pb age = 608.5 ± 0.4 Ma, Jackson et al., 2004) was used as a monitor of data quality during analyses. Concordia diagrams and weighted mean ages were produced using the program ISOPLOT/Ex 3.23 (Ludwig, 2003).

A.3. Major and trace element geochemistry

Major elements were analyzed on fused glass discs by X-ray fluorescence spectrometry at the National Research Center of Geoanalysis, Beijing and State Key Laboratory of Lithospheric Evolution, Institute of Geology and Geophysics, Chinese Academy of Sciences, Beijing. Trace elements (including REE) were determined by ICP–MS (VG Plasma Quad PQ2 Turbo ICP–MS and Finnigan MAT Element 2 high-resolution ICP–MS) at the State Key Laboratory of Lithospheric Evolution, Institute of Geology and Geophysics, Chinese Academy of Sciences, Beijing and the State Key Laboratory of Mineral Deposits Research, Nanjing University. About 100 mg whole-rock powders were dissolved in distilled HF-HNO_3 in Teflon screw-cap beakers and high-pressure Teflon bombs at 200 °C for 4 days, dried and then digested with HNO_3 at 150 °C for 1 day. Dissolved samples were diluted to 50 ml with 1% HNO_3 before analyses. A blank solution was prepared and the total procedural blank was <50 ng for all trace elements. Indium was used as an internal standard to correct for matrix effects and instrument drift. The Chinese national standards GSR-1 (granite) and GSR-3 (basalt) were used to monitor analyses. Errors for major element analysis are within 1%, except for P_2O_5 (5%), and analyses for most trace elements (including REE) are within 10%.

A.4. Rb–Sr and Sm–Nd isotopic analyses

Samples for Rb–Sr and Sm–Nd isotopic analyses were dissolved in Teflon bombs after being spiked with ^{84}Sr, ^{87}Rb, ^{150}Nd and ^{149}Sm tracers prior to HF+$HClO_4$ dissolution. Rb, Sr, Sm and Nd were separated using conventional ion exchange procedures and measured using a GV IsoProbe-T and a Finnigan MAT 262 multi-collector mass spectrometer at the Institute of Geology and Geophysics, Chinese Academy of Sciences, Beijing. Procedural blanks were <100 pg for Sm and Nd and <500 pg for Rb and Sr. $^{143}Nd/^{144}Nd$ was corrected for mass fractionation by normalization to $^{146}Nd/^{144}Nd = 0.7219$ and $^{87}Sr/^{86}Sr$ ratios normalized to $^{86}Sr/^{88}Sr = 0.1194$. Typical within-run precision (2σ) for Sr and Nd was estimated to be ±0.000015. The measured values for the JNDi-1 Nd standard and the NBS-987 Sr standard were $^{143}Nd/^{144}Nd = 0.512113 \pm 5$ (N = 5) and $^{87}Sr/^{86}Sr = 0.710269 \pm 19$ (N = 3) during the period of data acquisition, respectively. The USGS standard BCR-2, prepared using the same procedures as the samples, yielded Rb = 46.14, Sr = 328.4, $^{87}Rb/^{86}Sr = 0.4066$, $^{87}Sr/^{86}Sr = 0.705011 \pm 13$ (2σ), Sm = 6.58, Nd = 29.01, $^{147}Sm/^{144}Nd = 0.1373$ and $^{143}Nd/^{144}Nd = 0.512621 \pm 15$ (2σ).

A.5. In-situ Lu–Hf isotope analyses

In-situ Lu–Hf isotope analyses were performed using a Newwave UP213 laser-ablation microprobe attached to a Finnigan Neptune multi-collector ICP-MS at the Institute of Mineral Resources, Chinese Academy of Geological Sciences, Beijing, using techniques and analytical procedures described by Wu et al. (2006) and Hou et al. (2007). The spot diameter was 55 μm. The measured $^{176}Hf/^{177}Hf$ ratio on the standard zircon (GJ-1) was 0.282009 ± 0.000004 (N = 96), similar to the commonly accepted $^{176}Hf/^{177}Hf$ ratio of 0.282000 ± 0.000005 measured using the solution method (Morel et al., 2008). For the calculation of initial Hf isotope ratio, the decay constant for ^{176}Lu proposed by Söderlund et al. (2004) was used. For the calculation of $\varepsilon_{Hf}(t)$ values we have adopted the chondritic values of Blichert-Toft and Albarede (1998). Hf model ages (T_{DM} and T_{DM}^{C}) were calculated on the basis of the depleted mantle model described by Griffin et al. (2002) and Yang et al. (2006).

Appendix B. Description of zircon U–Pb results

B.1. Chifeng–Aohan

Seventeen spots on 17 zircon grains from the andesitic basalt sample 08260-1 near Louzidian south to Chifeng were analyzed by the LA–ICP–MS method, and most of them give concordant ages (Supplementary Table A2 in the ESM, Fig. 6A). Except for five discordant analyses (spots 01, 06, 08, 14, 16), the remaining analyses yield a weighted mean $^{206}Pb/^{238}U$ age of 347 ± 3 Ma (95% confidence, MSWD = 3.4, N = 12). Its zircons are irregular, broken fragments with weak oscillatory zoning (Fig. 5A) and are characterized by high Th/U ratios (0.39–0.99), which are very similar to those of zircons separated from mafic rocks (e.g., McLelland et al., 2004; Zhang et al., 2009c). Therefore, the mean age of 347 ± 3 Ma is interpreted as the eruption age of the andesitic basalt in the Louzidian area.

For the brecciated rhyolite sample 07D023-1 and the brecciated dacite sample 07D023-2 collected from the lower part of the volcanic sequences near Zhangjiayingzi northwest to Aohan, 15 spots on 15 zircon grains in each sample were measured by the LA–ICP–MS method, and most of them are concordant (Supplementary Table A2 in the ESM, Fig. 6B–C). Except for two discordant analyses (spots 08, 14), the remaining analyses of sample 07D023-1 yield a weighted mean $^{206}Pb/^{238}U$ age of 344 ± 3 Ma (95% confidence, MSWD = 1.9, N =13). Except for three discordant analyses (spots 03, 04, 05) and one slightly old analysis (spot 01), the remaining analyses of sample 07D023-2 yield a weighted mean $^{206}Pb/^{238}U$ age of 344 ± 4 Ma (95% confidence, MSWD = 3.2, N = 11). Their zircons are characterized by well-developed oscillatory zoning (Fig. 5B–C) and high Th/U ratios (0.66–2.16), indicating a magmatic origin. Therefore, their weighted mean $^{206}Pb/^{238}U$ ages reflect eruption of the volcanic rocks from the lower part of the volcanic sequences northwest to Aohan at ca. 344 Ma during the Early Carboniferous.

Fifteen spots on 15 grains from the rhyolitic tuffaceous schist sample 08197-1 near the Xar Moron River north to Chifeng were analyzed by the LA–ICP–MS method, and most of them give concordant ages (Supplementary Table A2 in the ESM, Fig. 6D). Except for one discordant analysis (spot 14) and two inherited analyses (spots 06, 08), the remaining analyses yield a weighted mean $^{206}Pb/^{238}U$ age of 314 ± 3 Ma (95% confidence, MSWD = 2.9, N = 13). Their long or short euhedral prismatic morphology, high Th/U ratios (0.40–1.23) and oscillatory zoning (Fig. 5D) indicate that they are magmatic in origin. Therefore, the mean age of 314 ± 3 Ma is interpreted as the eruption age of the rhyolitic tuffaceous schist near the Xar Moron River north to Chifeng.

For the dacite sample 07D016-1 collected from the upper part of the volcanic sequences near Halagou northwest to Aohan, 30 spots on 30 zircon grains were measured by the LA–ICP–MS method, and most of them are concordant (Supplementary Table A2 in the ESM, Fig. 6E). Except for three discordant analyses (spots 01, 18, 24), the remaining analyses yield a weighted mean $^{206}Pb/^{238}U$ age of 258 ± 1 Ma (95% confidence, MSWD = 2.1, N = 27). Their long or short euhedral prismatic morphology, high Th/U ratios (0.51–0.78) and oscillatory zoning (Fig. 5F) indicate that they are magmatic in origin. Therefore, the mean age of 258 ± 1 Ma is interpreted as the eruption age of the dacite from the upper part of the volcanic sequences near Halagou northwest to Aohan.

Sixteen spots on 16 grains from the andesite sample 07D024-1 near Zhangjiayingzi northwest to Aohan were measured by SHRIMP, and most of them are concordant (Supplementary Table A1 in the ESM, Fig. 6F). They exhibit a very complex age distribution with abundant inheritance. One concordant analysis (spot 7.1) yields an old inherited $^{207}Pb/^{206}Pb$ age of 2479 ± 18 Ma, similar to the ages of the basement rocks in the NCC. Two concordant inherited analyses (spots 2.1, 15.1) yield a weighted mean $^{206}Pb/^{238}U$ age of 497 ± 9 Ma (95% confidence, MSWD = 0.106), similar to the Early Paleozoic volcanic rocks from the Bainaimiao arc belt (Zhang et al., 2014). Eight concordant inherited analyses (spots 1.1, 4.1, 8.1, 9.1, 10.1, 12.1, 13.1, 14.1) yield a weighted mean $^{206}Pb/^{238}U$ age of 357 ± 9 Ma (95% confidence, MSWD = 4.5). Except for the above inherited analyses and three discordant analyses (spots 3.1, 6.1, 16.1), the remaining analyses (spots 5.1, 11.1) yield a weighted mean $^{206}Pb/^{238}U$ age of 273 ± 6 Ma (95% confidence, MSWD = 0.031, N = 2). Their high Th/U ratios (0.31–1.12) and oscillatory zoning (Fig. 5E) indicate a magmatic in origin. Therefore, the weighted mean $^{206}Pb/^{238}U$ age of 273 ± 6 Ma is interpreted as the eruption age of the pyroxene andesite near Zhangjiayingzi northwest to Aohan.

For the dacitic tuffaceous schist sample 07D033-1 collected from Xiaowudetu north to Chifeng, 16 spots on 16 grains were measured by the LA–ICP–MS method (Supplementary Table A2 in the ESM, Fig. 6G). Except for three inherited analyses (spots 10, 14, 16) and two exotic young grains (spots 02, 07), the remaining analyses yield a weighted mean $^{206}Pb/^{238}U$ age of 261 ± 3 Ma (95% confidence, MSWD = 2.5, N = 11). Their long or short euhedral prismatic morphology, high Th/U ratios (0.53–1.66) and oscillatory zoning (Fig. 5G) indicate that they are magmatic in origin. Therefore, the weighted mean $^{206}Pb/^{238}U$ age of 261 ± 3 Ma reflects the eruption age of the tuffaceous schist near Xiaowudetu north to Chifeng.

Sixteen spots on 16 grains from the rhyolitic tuff sample 07D037-1 near Dingjiawopu northwest to Chifeng were measured by the LA–ICP–MS method, and most of them are concordant (Supplementary Table A2 in the ESM, Fig. 6H). Except for two discordant analyses (spots 01, 13), the remaining analyses yield a weighted mean $^{206}Pb/^{238}U$ age of 273 ± 5 Ma (95% confidence, MSWD = 6.1, N =14). Its zircons are characterized by long or short euhedral prismatic morphology, well-developed oscillatory zoning (Fig. 5H) and high Th/U ratios (0.61–1.27), indicating a magmatic origin. Therefore, the weighted mean $^{206}Pb/^{238}U$ age of 261 ± 3 Ma reflects the eruption age of the rhyolitic tuff near Dingjiawopu northwest to Chifeng.

B.2. Sanjingquan, Siziwangqi

Thirty-one spots on 28 grains from the rhyolitic tuff sample 07057-1 near Sanjingquan were measured by the LA–ICP–MS method, and most of them are concordant (Supplementary Table A2 in the ESM, Fig. 6I). Except for two discordant analyses (spots 07, 08), the remaining analyses yield a weighted mean $^{206}Pb/^{238}U$ age of 276 ± 2 Ma (95% confidence, MSWD = 3.8, N = 29). Their long or short euhedral prismatic morphology, high Th/U ratios (0.24–1.10) and oscillatory zoning (Fig. 5I) indicate that they are magmatic in origin. Therefore, the weighted mean $^{206}Pb/^{238}U$ age of 276 ± 2 Ma reflects the eruption age of the rhyolitic tuff near Sanjingquan, Siziwangqi during the Early Permian.

B.3. Damaoqi–Bayan Obo

For the basaltic andesite sample 07125-1 collected near Huxiye northeast to Damaoqi, 18 pots on 18 grains were measured by SHRIMP (Supplementary Table A1 in the ESM, Fig. 6J). One concordant analysis (spot 4.1) yields an old inherited $^{207}Pb/^{206}Pb$ age of 1946 ± 15 Ma. One analysis (spot 8.1) exhibits very large errors due to low U concentration. Except for above two analyses and three exotic young grains (spots 1.1, 5.1, 7.1), the remaining analyses yield a weighted mean $^{206}Pb/^{238}U$ age of 278 ± 5 Ma (95% confidence, MSWD = 3.4, N = 13). Their long or short euhedral prismatic morphology, high Th/U ratios (0.19–1.03) and oscillatory zoning (Fig. 5J) indicate that they are magmatic in origin. Therefore, the weighted mean $^{206}Pb/^{238}U$ age of 278 ± 5 Ma is interpreted as the eruption age of the basaltic andesite near Huxiye northeast to Damaoqi.

Fifteen spots on 15 grains from the rhyolite sample 08485-1 near Baiyanhua northeast to Damaoqi were measured by the LA–ICP–MS method, and most of them are concordant (Supplementary Table A2 in the ESM, Fig. 6K). Except for two discordant analyses (spots 02, 14), the remaining analyses yield a weighted mean $^{206}Pb/^{238}U$ age of 264 ± 2 Ma (95% confidence, MSWD = 0.58, N = 13). Their long or short euhedral prismatic morphology, high Th/U ratios (0.55–0.81) and oscillatory zoning (Fig. 5K) indicate that they are magmatic in origin. Therefore, the weighted mean $^{206}Pb/^{238}U$ age of 264 ± 2 Ma reflects the eruption age of the rhyolite near Baiyanhua northeast to Damaoqi.

For the rhyolite sample 08543-2 collected from Bayinaobao Sum northwest to Damaoqi, 15 spots on 15 grains were measured by the LA–ICP–MS method, and all of them are concordant (Supplementary Table A2 in the ESM, Fig. 6L). Their weighted mean $^{206}Pb/^{238}U$ age is 269 ± 3 Ma (95% confidence, MSWD = 4.5, N = 15). Its zircons are characterized by long or short euhedral prismatic morphology, well-developed oscillatory zoning (Fig. 5L) and high Th/U ratios (0.56–0.84), indicating a magmatic origin. Therefore, the weighted mean

$^{206}Pb/^{238}U$ age of 269 ± 3 Ma reflects the eruption age of the rhyolite near Bayinaobao Sum northwest to Damaoqi.

Fifteen spots on 15 grains from the andesite sample 08550-1 near Agui northeast to Bayan Obo were measured by the LA–ICP–MS method (Supplementary Table A2 in the ESM, Fig. 6M). Except for one inherited grains (spot 13) and three discordant analyses (spots 06, 07, 14), the remaining analyses yield a weighted mean $^{206}Pb/^{238}U$ age of 273 ± 3 Ma (95% confidence, MSWD = 2.2, N = 11). Their long or short euhedral prismatic morphology, high Th/U ratios (0.31–0.81) and oscillatory zoning (Fig. 5M) indicate that they are magmatic in origin. Therefore, the weighted mean $^{206}Pb/^{238}U$ age of 273 ± 3 Ma reflects the eruption age of the andesite near Agui northeast to Bayan Obo.

For the rhyolitic porphyry samples 07116-1 and 07117-1 collected from Chaganaobao Sumu northeast to Damaoqi, they were analyzed by SHRIMP (Supplementary Table A1 in the ESM). Nine spots on 9 grains from sample 07116-1 were measured and all of them are concordant (Fig. 6N). They yield a weighted mean $^{206}Pb/^{238}U$ age of 261 ± 2 Ma (95% confidence, MSWD = 0.65, N = 9). Nineteen spots on 19 grains from sample 07117-1 were measured and most of them are concordant (Fig. 6O). Five concordant inherited analyses (spots 3.1, 4.1, 5.1, 12.1, 14.1) yield a weighted mean $^{206}Pb/^{238}U$ age of 434 ± 13 Ma (95% confidence, MSWD = 3.4). Except for the above inherited grains and two discordant analyses (spots 2.1, 6.1), the remaining analyses yield a weighted mean $^{206}Pb/^{238}U$ age of 261 ± 3 Ma (95% confidence, MSWD = 2.5, N = 12), which is almost the same as that obtained from sample 07116-1. Both zircons from samples 07116-1 and 07117-1 are characterized by long or short euhedral prismatic morphology, well-developed oscillatory zoning (Fig. 5N–O) and high Th/U ratios (0.19–0.90), indicating that they are magmatic in origin. Therefore, formation of the rhyolitic porphyries near Chaganaobao Sumu northeast to Damaoqi occurred during the Middle Permian at ca. 261 Ma.

Appendix C. Supplementary data

Supplementary data to this article can be found online at http://dx.doi.org/10.1016/j.lithos.2015.11.027.

References

Annen, C., Blundy, J.D., Sparks, R.S.J., 2006. The genesis of intermediate and silicic magmas in deep crustal hot zones. Journal of Petrology 47, 505–539.

Bai, X., Liu, S., Wang, W., Yang, P., Li, Q., 2013. U–Pb geochronology and Lu–Hf isotopes of zircons from newly identified Permian–Early Triassic plutons in western Liaoning province along the northern margin of the North China Craton: constraints on petrogenesis and tectonic setting. International Journal of Earth Sciences 102, 671–685.

Black, L.P., Kamo, S.L., Allen, C.M., Aleinikoff, J.N., Davis, D.W., Korsch, R.J., Foudoulis, C., 2003. TEMORA 1: a new zircon standard for Phanerozoic U–Pb geochronology. Chemical Geology 200, 155–170.

Blichert-Toft, J., Albarede, F., 1998. The Lu–Hf isotope geochemistry of chondrites and the evolution of the mantle–crust system. Earth and Planetary Science Letters 148, 243–258.

Boardman, S.J., Condie, K.C., 1986. Early Proterozoic bimodal volcanic rocks in central Colorado, U.S.A., Part II: geochemistry, petrogenesis and tectonic setting. Precambrian Research 34, 37–68.

Briqueu, L., Bougault, H., Joron, J.L., 1984. Quantification of Nb, Ta, Ti and V anomalies in magmas associated with subduction zones: petrogenetic implications. Earth and Planetary Science Letters 68, 297–308.

Bureau of Geology and Mineral Resources of Inner Mongolia (BGMRIM), 1967. Geological map of Chifeng (K-50-XVII), Hohhot, Bureau of Geology and Mineral Resources of Inner Mongolia, scale 1:200000 (in Chinese).

BGMRIM, 1970. Geological map of Aohanqi (K-50-XVIII), Hohhot, Bureau of Geology and Mineral Resources of Inner Mongolia, scale 1:200000 (in Chinese).

BGMRIM, 1971a. Geological map of Bayan Obo (K-49-XX), Hohhot, Bureau of Geology and Mineral Resources of Inner Mongolia, scale 1:200000 (in Chinese).

BGMRIM, 1971b. Geological map of Damaoqi (K-49-XXI), Hohhot, Bureau of Geology and Mineral Resources of Inner Mongolia, scale 1:200000 (in Chinese).

BGMRIM, 1972. Geological map of Sandaogou (K-49-XXIII), Hohhot, Bureau of Geology and Mineral Resources of Inner Mongolia, scale 1:200000 (in Chinese).

BGMRIM, 1976. Geological map of Xianghuangqi (K-49-XVIII), Hohhot, Bureau of Geology and Mineral Resources of Inner Mongolia, scale 1:200000 (in Chinese).

BGMRIM, 1991. Regional Geology of Inner Mongolia Autonomous Region. Geological Publishing House, Beijing (725 pp., (in Chinese with English abstract)).

Bureau of Geology and Mineral Resources of Liaoning Province (BGMRLP), 1971. Geological maps of Keshiketengqi (K-50-X) and Wufendi (K-50-XI), Shenyang, Bureau of Geology and Mineral Resources of Liaoning Province, scale 1:200000 (in Chinese).

Cope, T.D., Ritts, B.D., Darby, B.J., Fildani, A., Graham, S.A., 2005. Late Paleozoic sedimentation on the northern margin of the North China block: implications for regional tectonics and climate change. International Geology Review 47, 270–296.

Davidson, J.P., McMillan, N.J., Moorbath, S., Wörner, G., Harmon, R.S., Lopez-Escobar, L., 1990. The Nevados de Payachata volcanic region (18° S/69° W, N. Chile) II. Evidence for widespread crustal involvement in Andean magmatism. Contributions to Mineralogy and Petrology 105, 412–432.

Ducea, M.N., Saleeby, J.B., Bergantz, G., 2015. The architecture, chemistry, and evolution of continental magmatic arcs. Annual Review of Earth and Planetary Sciences 43, 299–331.

Ersoy, Y., Helvacı, C., Sözbilir, H., Erkül, F., Bozkurt, E., 2008. A geochemical approach to Neogene–Quaternary volcanic activity of western Anatolia: an example of episodic bimodal volcanism within the Selendi Basin, Turkey. Chemical Geology 255, 265–282.

Feeley, T.C., Dungan, M.A., Frey, F.A., 1998. Geochemical constraints on the origin of mafic and silicic magmas at Cordon El Guadal, Tatara-San Pedro Complex, central Chile. Contributions to Mineralogy and Petrology 131, 393–411.

Feng, Y.G., Liu, S.W., Lü, Y.J., Tian, W., Liu, X.M., 2009. Petrogenesis of the Late Paleozoic diorites-granitoids in Fengshan area, northern Hebei Province: constraints from petrochemistry, zircon U–Pb chronology and Hf isotope. Acta Scientiarum Naturalium Universitatis Pekinensis 45, 59–70 (in Chinese with English abstract).

Folkes, C.B., de Silva, S.L., Wright, H.M., Cas, R.A.F., 2011. Geochemical homogeneity of a long-lived, large silicic system; evidence from the Cerro Galán caldera, NW Argentina. Bulletin of Volcanology 73, 1455–1486.

Gómez-Tuena, A., LaGatta, A.B., Langmuir, C.H., Goldstein, S.L., Ortega-Gutiérrez, F., Carrasco-Núñez, G., 2003. Temporal control of subduction magmatism in the eastern Trans-Mexican Volcanic Belt: mantle sources, slab contributions, and crustal contamination. Geochemistry Geophysics Geosystems 4, 8912. http://dx.doi.org/10.1029/2003GC000524.

Gómez-Tuena, A., Orozco-Esquivel, M.T., Ferrari, L., 2007. Igneous petrogenesis of the Trans-Mexican Volcanic Belt. In: Alaniz-Álvaers, S.A., Nieto-Samaniego, Á.F. (Eds.), Geology of México: Celebrating the Centenary of the Geological Society of México. Geological Society of America Special Papers 422, pp. 129–181.

Gómez-Tuena, A., Straub, S.M., Zellmer, G.F., 2014. An introduction to orogenic andesites and crustal growth. In: Gómez-Tuena, A., Straub, S.M., Zellmer, G.F. (Eds.), Orogenic Andesites and Crustal Growth. Geological Society, London, Special Publications 385, pp. 1–13.

Griffin, W.L., Wang, X., Jackson, S.E., Pearson, S.E., O'Reilly, S.Y., Xu, X.S., Zhou, X.M., 2002. Zircon chemistry and magma genesis, SE China: in-situ analysis of Hf isotopes, Tonglu and Pingtan igneous complexes. Lithos 61, 237–269.

Hart, G.L., Johnson, C.M., Shirey, S.B., Clynne, M.A., 2002. Osmium isotope constraints on lower crustal recycling and pluton preservation at Lassen Volcanic Center, CA. Earth and Planetary Science Letters 199, 269–285.

Haschke, M., Günther, A., Melnick, D., Echtler, H., Reutter, K.-J., Scheuber, E., Oncken, O., 2006. Central and southern Andean tectonic evolution inferred from arc magmatism. In: Oncken, O., Chong, G., Franz, G., Giese, P., Götze, H.-J., Ramos, V.A., Strecker, M.R., Wigger, P. (Eds.), The Andes: Active Subduction Orogeny. Frontiers in Earth Science Series. Springer-Verlag, Berlin, pp. 337–353.

Hildreth, W., Moorbath, S., 1988. Crustal contributions to arc magmatism in the Andes of central Chile. Contributions to Mineralogy and Petrology 455–489.

Hou, K.J., Li, Y.H., Zou, T.R., Qu, X.M., Shi, Y.R., Xie, G.Q., 2007. Laser ablation–MC–ICP–MS technique for Hf isotope microanalysis of zircon and its geological applications. Acta Petrologica Sinica 23, 2595–2604 (in Chinese with English abstract).

Hsu, K.J., Wang, Q., Hao, J., 1991. Geologic evolution of the Neomonides: a working hypothesis. Eclogae Geologicae Helvetiae 84, 1–31.

Hu, Z.C., Gao, S., Liu, Y.S., Hu, S.H., Chen, H.H., Yuan, H.L., 2008. Signal enhancement in laser ablation ICP–MS by addition of nitrogen in the central channel gas. Journal of Analytical Atomic Spectrometry 23, 1093–1101.

Inner Mongolia Institute of Geology Survey (IMIGS), 2003. Geological map of Bayan Obo (K49C003002), Hohhot, Bureau of Geology and Mineral Resources of Inner Mongolia, scale 1:250000 (in Chinese).

Jackson, S.E., Pearson, N.J., Griffin, W.L., Belousova, E.A., 2004. The application of laser ablation–inductively coupled plasma–mass spectrometry to in situ U–Pb zircon geochronology. Chemical Geology 21, 47–69.

Jagoutz, O., Kelemen, P.B., 2015. Role of arc processes in the formation of continental crust. Annual Review of Earth and Planetary Sciences 43, 363–404.

Jahn, B.M., Condie, K.C., 1995. Evolution of the Kaapvaal Craton as viewed from geochemical and Sm–Nd isotopic analyses of intracratonic pelites. Geochimica et Cosmochimica Acta 59, 549–555.

Jahn, B.M., Wu, F.Y., Chen, B., 2000. Massive granitoid generation in Central Asia: Nd isotope evidence and implication for continental growth in the Phanerozoic. Episodes 23, 82–92.

Jicha, B.R., Singer, B.S., Beard, B.L., Johnson, C.M., Moreno-Roa, H., Naranjo, J.A., 2007. Rapid magma ascent and generation of ^{230}Th excesses in the lower crust at Puyehue–Cordón Caulle, Southern Volcanic Zone, Chile. Earth and Planetary Science Letters 255, 229–242.

Kay, S.M., Gordillo, C.E., 1994. Pocho volcanic rocks and the melting of depleted continental lithosphere above a shallowly dipping subduction zone in the central Andes. Contributions to Mineralogy and Petrology 117, 25–44.

Kay, S.M., Godoy, E., Kurtz, A., 2005. Episodic arc migration, crustal thickening, subduction erosion, and magmatism in the south-central Andes. Geological Society of America Bulletin 117, 67–88.

Kleine, T., Mezger, K., Zimmermann, U., Münker, C., Bahlburg, H., 2004. Crustal evolution along the Early Ordovician proto-Andean margin of Gondwana: trace element and isotope evidence from the Complejo Igneo Pocitos (Northwest Argentina). The Journal of Geology 112, 503–520.

Lackey, J.S., Valley, J.W., Saleeby, J.B., 2005. Supracrustal input to magmas in the deep crust of Sierra Nevada Batholith: evidence from high-$\delta^{18}O$ zircon. Earth and Planetary Science Letters 235, 315–330.
Lake, E.T., Farmer, G.L., 2015. Oligo-Miocene mafic intrusions of the San Juan Volcanic Field, southwestern Colorado, and their relationship to voluminous, caldera-forming magmas. Geochimica et Cosmochimica Acta 157, 86–108.
Lee, C.-T.A., Bachmann, O., 2014. How important is the role of crystal fractionation in making intermediate magmas? Insights from Zr and P systematics. Earth and Planetary Science Letters 393, 266–274.
Li, J.Y., 2006. Permian geodynamic setting of Northeast China and adjacent regions: closure of the Paleo-Asian Ocean and subduction of the Paleo-Pacific Plate. Journal of Asian Earth Sciences 26, 207–224.
Li, J.-X., Qin, K.-Z., Li, G.-M., Richards, J.P., Zhao, J.-X., Cao, M.-J., 2014. Geochronology, geochemistry, and zircon Hf isotopic compositions of Mesozoic intermediate-felsic intrusions in central Tibet: petrogenetic and tectonic implications. Lithos 198–199, 77–91.
Liu, Y.S., Hu, Z.C., Gao, S., Günther, D., Xu, J., Gao, C.G., Chen, H.H., 2008. In situ analysis of major and trace elements of anhydrous minerals by LA–ICP–MS without applying an internal standard. Chemical Geology 257, 34–43.
Liu, Y.S., Gao, S., Hu, Z.C., Gao, C.G., Zong, K.Q., Wang, D.B., 2010a. Continental and oceanic crust recycling-induced melt-peridotite interactions in the Trans-North China orogen: U–Pb dating, Hf isotopes and trace elements in zircons from mantle xenoliths. Journal of Petrology 51, 537–571.
Liu, Y.S., Hu, Z.C., Zong, K.Q., Gao, C.G., Gao, S., Xu, J., Chen, H.H., 2010b. Reappraisement and refinement of zircon U–Pb isotope and trace element analyses by LA–ICP–MS. Chinese Science Bulletin 55, 1535–1546.
Liu, J., Zhao, Y., Liu, X., Wang, Y., Liu, X., 2012. Early Jurassic rapid exhumation of the basement rocks along the northern margin of the North China Craton: evidence from the Xiabancheng basin in the Yanshan Tectonic Belt. Basin Research 24, 544–558.
Liu, C., Liu, W., Zhou, Z., 2014. Geochronology, geochemistry and tectonic setting of the Paleozoic–Early Mesozoic intrusive in Siziwangqi, Inner Mongolia. Acta Geologica Sinica 88, 992–1002 (in Chinese with English abstract).
Lucassen, F., Kramer, W., Bartsch, V., Wilke, H.-G., Franz, G., Romer, R.L., Dulski, P., 2006. Nd, Pb, and Sr isotope composition of juvenile magmatism in the Mesozoic large magmatic province of northern Chile (18–27°S): indications for a uniform subarc mantle. Contributions to Mineralogy and Petrology 152, 571–589.
Ludwig, K.R., 2001. SQUID 1.02: a user's manual. Special Publication No. 2. Berkeley Geochronology Center, Berkeley, California (19 pp.).
Ludwig, K.R., 2003. User's manual for Isoplot 3.00. A geochronological Toolkit for Microsoft Excel. Special Publication No. 4a. Berkeley Geochronology Center, Berkeley, California (70 pp.).
Luo, H., Wu, T., Zhao, L., He, Y., Jin, X., 2009. Permian high Ba–Sr granitoids: geochemistry, age and tectonic implications of Erlangshan pluton, Urad Zhongqi, Inner Mongolia. Acta Geologica Sinica 83, 603–614.
Ma, X., Chen, B., Chen, J.F., Niu, X.L., 2013. Zircon SHRIMP U–Pb age, geochemical, Sr–Nd isotopic, and in-situ Hf isotopic data of the Late Carboniferous–Early Permian plutons in the northern margin of the North China Craton. Science China: Earth Sciences 56, 126–144.
Mamani, M., Wörner, G., Sempere, T., 2010. Geochemical variations in igneous rocks of the Central Andean orocline (13°S to 18°S): tracing crustal thickening and magma generation through time and space. Geological Society of America Bulletin 122, 162–182.
Matteini, M., Mazzuoli, R., Omarini, R., Cas, R., Maas, R., 2002. The geochemical variations of the upper Cenozoic volcanism along the Calama–Olacapato–El Toro transversal fault system in central Andes (~24°S): petrogenetic and geodynamic implications. Tectonophysics 345, 211–227.
McLelland, J., Bickford, M.E., Hill, B.M., Clechenko, C.C., Valley, J.W., Hamilton, M.A., 2004. Direct dating of Adirondack massif anorthosite by U–Pb SHRIMP analysis of igneous zircon: implications for AMCG complexes. Geological Society of America Bulletin 116, 1299–1317.
McMillan, N.J., Harmon, R.S., Moorbath, S., Lopez-Escobar, L., Strong, D.F., 1989. Crustal sources involved in continental arc magmatism: a case study of volcan Mocho-Choshuenco, southern Chile. Geology 17, 1152–1156.
Miao, L.C., Fan, W.M., Liu, D.Y., Zhang, F.Q., Shi, Y.R., Guo, F., 2008. Geochronology and geochemistry of the Hegenshan ophiolitic complex: implications for late-stage tectonic evolution of the Inner Mongolia-Daxinganling Orogenic Belt, China. Journal of Asian Earth Sciences 32, 348–370.
Morel, M.L.A., Nebel, O., Nebel-Jacobsen, Y.J., Miller, J.S., Vroon, P.Z., 2008. Hafnium isotope characterization of the GJ-1 zircon reference material by solution and laser–ablation MC–ICPMS. Chemical Geology 255, 231–235.
Mtoro, M., Maboko, M.A.H., Manya, S., 2009. Geochemistry and geochronology of the bimodal volcanic rocks of the Suguti area in the southern part of the Musoma-Mara Greenstone Belt, Northern Tanzania. Precambrian Research 174, 241–257.
Muñoz, M., Charrier, R., Fanning, C.M., Maksaev, V., Deckart, K., 2012. Zircon trace element and O–Hf isotope analyses of mineralized intrusions from El Teniente ore deposit, Chilean Andes: constraints on the source and magmatic evolution of porphyry Cu–Mo related magmas. Journal of Petrology 53, 1091–1122.
Murphy, J.B., 2006. Arc magmatism I: relationship between tectonic evolution and petrogenesis. Geoscience Canada 33, 145–216.
Murphy, J.B., 2007. Arc magmatism II: geochemical and isotopic characteristics. Geoscience Canada 34, 7–35.
Nasdala, L., Hofmeister, W., Norberg, N., Mattinson, J.M., Corfu, F., Dörr, W., Kamo, S.L., Kennedy, A.K., Kronz, A., Reiners, P.W., Frei, D., Kosler, J., Wan, Y., Götze, J., Häger, T., Kröner, A., Valley, J.W., 2008. Zircon M257— a homogeneous natural reference material for the ion microprobe U–Pb analysis of zircon. Geostandards and Geoanalytical Research 32, 247–265.
Ort, M.H., Coira, B.L., Mazzoni, M.M., 1996. Generation of a crust-mantle magma mixture: magma sources and contamination at Cerro Panizos, central Andes. Contributions to Mineralogy and Petrology 123, 308–322.
Ramos, V.A., 1999. Plate tectonic setting of the Andean Cordillera. Episodes 22, 183–190.
Richards, J.P., 2003. Tectono-magmatic precursors for porphyry Cu–(Mo–Au) deposit formation. Economic Geology 98, 1515–1533.
Richards, J.P., 2005. Cumulative factors in the generation of giant calc-alkaline porphyry Cu deposits. In: Porter, T.M. (Ed.), Super-Porphyry Copper & Gold Deposits: A Global Perspective. PGC Publishing, Adelaide, pp. 7–25.
Riley, T.R., Leat, P.T., Pankhurst, R.J., Harris, C., 2001. Origins of large volume rhyolitic volcanism in the Antarctic Peninsula and Patagonia by crustal melting. Journal of Petrology 42, 1043–1065.
Robinson, P.T., Zhou, M.F., Hu, X.F., Reynolds, P., Bai, W., Yang, J., 1999. Geochemical constraints on the origin of the Hegenshan Ophiolite, Inner Mongolia, China. Journal of Asian Earth Sciences 17, 423–442.
Rogers, G., Hawkesworth, C.J., 1989. A geochemical traverse across the North Chilean Andes: evidence for crustal generation from the mantle wedge. Earth and Planetary Science Letters 91, 271–285.
Rudnick, R.L., 1995. Making continental crust. Nature 378, 571–578.
Rudnick, R.L., Gao, S., 2003. Composition of the continental crust. In: Rudnick, R.L. (Ed.), Treatise on GeochemistryThe Crust 3. Pergamon, Oxford, UK, pp. 1–64.
Sengör, A.M.C., Natal'in, B.A., Burtman, V.S., 1993. Evolution of the Altaid tectonic collage and Paleozoic crustal growth in Eurasia. Nature 364, 299–307.
de Silva, S.L., Riggs, N.R., Barth, A.P., 2015. Quickening the pulse: fractal tempos in continental arc magmatism. Element 11, 113–118.
Söderlund, U., Patchett, P.J., Vervoort, J.D., Isachsen, C.E., 2004. The ^{176}Lu decay constant determined by Lu–Hf and U–Pb isotope systematics of Precambrian mafic intrusions. Earth and Planetary Science Letters 219, 311–324.
Solano, J.M.S., Jackson, M.D., Sparks, R.S.J., Blundy, J.D., Annen, C., 2012. Melt segregation in deep crustal hot zones: a mechanism for chemical differentiation, crustal assimilation and the formation of evolved magmas. Journal of Petrology 53, 1999–2026.
Stern, C.R., Kilian, R., 1996. Role of the subducted slab, mantle wedge and continental crust in the generation of adakites from the Andean Austral Volcanic Zone. Contributions to Mineralogy and Petrology 123, 263–281.
Sun, S.S., McDonough, W.F., 1989. Chemical and isotopic systematics of oceanic basalts: implications for mantle composition and processes. In: Sauders, A.D., Norry, M.J. (Eds.), Magmatism in the Ocean Basins. Geological Society Special Publication 42, pp. 313–345.
Tassara, A., 2006. Factors controlling the crustal density structure underneath active continental margins with implications for their evolution. Geochememistry Geophysics Geosystems 7, Q01001. http://dx.doi.org/10.1029/2005GC001040.
Taylor, S.R., McLennan, S.M., 1985. The Continental Crust: Its Composition and Evolution. Blackwell Science Publication, Oxford (312 pp.).
Wang, Q., Liu, X.Y., 1986. Paleoplate tectonics between Cathaysia and Angaraland in Inner Mongolia of China. Tectonics 5, 1073–1088.
Wang, H.C., Zhao, F.Q., Li, H.M., Sun, L.X., Miao, L.C., Ji, S.P., 2007. Zircon SHRIMP U–Pb age of the dioritic rocks from northern Hebei: the geological records of late Paleozoic magmatic arc. Acta Petrologica Sinica 23, 597–604 (in Chinese with English abstract).
Wang, F., Chen, F.K., Hou, Z.H., Peng, P., Zhai, M.G., 2009. Zircon ages and Sr–Nd–Hf isotopic composition of late Paleozoic granitoids in the Chongli–Chicheng area, northern margin of the North China block. Acta Petrologica Sinica 25, 3057–3074 (in Chinese with English abstract).
Williams, I.S., 1998. U–Th–Pb geochronology by ion microprobe. In: McKibben, M.A., Shanks, W.C.I.I.I., Ridley, W.I. (Eds.), Applications of Microanalytical Techniques to Understanding Mineralizing Processes. Review in Economic Geology 7, pp. 1–35.
Wilson, M., 1989. Igneous Petrogenesis: A Global Tectonic Approach. Chapman & Hall, London (466 pp.).
Winchester, J.A., Floyd, P.A., 1977. Geochemical discrimination of different magma series and their differentiation products. Chemical Geology 20, 325–343.
Wörner, G., Moorbath, S., Horn, S., Entenmann, J., Harmon, R.S., Davidson, J.P., López-Escobar, L., 1994. Large- and fine-scale geochemical variations along the Andean Arc of Northern Chile (17.5°–22°S). In: Reutter, K.J., Scheuber, E., Wigger, P.J. (Eds.), Tectonics of the Southern Central Andes, Structure and Evolution of an Active Continental Margin. Springer Verlag, Berlin, pp. 77–91.
Wu, F.Y., Yang, Y.H., Xie, L.W., Yang, J.H., Xu, P., 2006. Hf isotopic compositions of the standard zircons and baddeleyites used in U–Pb geochronology. Chemical Geology 234, 105–126.
Xiao, W., Windley, B.F., Hao, J., Zhai, M.G., 2003. Accretion leading to collision and the Permian Solonker suture, Inner Mongolia, China: termination of the central Asian orogenic belt. Tectonics 22, 1069. http://dx.doi.org/10.1029/2002TC001484.
Xiao, W.J., Windley, B.F., Huang, B.C., Han, C.M., Yuan, C., Chen, H.L., Sun, M., Sun, S., Li, J.L., 2009. End-Permian to mid-Triassic termination of the accretionary processes of the southern Altaids: implications for the geodynamic evolution, Phanerozoic continental growth, and metallogeny of Central Asia. International Journal of Earth Sciences 98, 1189–1217.
Yang, J.H., Wu, F.Y., Shao, J.A., Wilde, S.A., Xie, L.W., Liu, X.M., 2006. Constraints on the timing of uplift of the Yanshan Fold and Thrust Belt, North China. Earth and Planetary Science Letters 246, 336–352.
Ye, H., Zhang, S.H., Zhao, Y., Liu, J.M., He, Z.F., 2014. Recognition of the latest Devonian volcanic rocks in the Chifeng area, northern North China block and its geological implications. Geological Bulletin of China 33, 1274–1283 (in Chinese with English abstract).
Yuan, H.L., Gao, S., Liu, X.M., Li, H.M., Günther, D., Wu, F.Y., 2004. Accurate U–Pb age and trace element determinations of zircon by laser ablation inductively coupled plasma mass spectrometry. Geostandards and Geoanalytical Research 28, 353–370.

Zhang, S.H., Zhao, Y., Song, B., Wu, H., 2004. The Late Paleozoic gneissic granodiorite pluton in Early Precambrian high-grade metamorphic terrains near Longhua County in northern Hebei Province, North China: result from zircon SHRIMP U–Pb dating and its tectonic implications. Acta Petrologica Sinica 20, 621–626 (in Chinese with English abstract).

Zhang, S.H., Zhao, Y., Song, B., 2006. Hornblende thermobarometry of the Carboniferous granitoids from the Inner Mongolia Paleo-uplift: implications for the tectonic evolution of the northern margin of North China block. Mineralogy and Petrology 87, 123–141.

Zhang, S.H., Zhao, Y., Song, B., Yang, Z.Y., Hu, J.M., Wu, H., 2007a. Carboniferous granitic plutons from the northern margin of the North China block: Implications for a Late Paleozoic active continental margin. Journal of the Geological Society London 164, 451–463.

Zhang, S.H., Zhao, Y., Song, B., Yang, Y.H., 2007b. Zircon SHRIMP U–Pb and in-situ Lu–Hf isotope analyses of a tuff from Western Beijing: evidence for missing late Paleozoic arc volcano eruptions at the northern margin of the North China block. Gondwana Research 12, 157–165.

Zhang, X., Zhang, H., Tang, Y., Wilde, S.A., Hu, Z., 2008. Geochemistry of Permian bimodal volcanic rocks from central Inner Mongolia, North China: implication for tectonic setting and Phanerozoic continental growth in Central Asian Orogenic Belt. Chemical Geology 249, 262–281.

Zhang, S.H., Zhao, Y., Song, B., Hu, J.M., Liu, S.W., Yang, Y.H., Chen, F.K., Liu, X.M., Liu, J., 2009a. Contrasting Late Carboniferous and Late Permian-Middle Triassic intrusive suites from the northern margin of the North China craton: geochronology, petrogenesis and tectonic implications. Geological Society of America Bulletin 121, 181–200.

Zhang, S.H., Zhao, Y., Kröner, A., Liu, X.M., Xie, L.W., Chen, F.K., 2009b. Early Permian plutons from the northern North China Block: constraints on continental arc evolution and convergent margin magmatism related to the Central Asian Orogenic Belt. International Journal of Earth Sciences 98, 1441–1467.

Zhang, S.H., Zhao, Y., Liu, X.C., Liu, D.Y., Chen, F., Xie, L.W., Chen, H.H., 2009c. Late Paleozoic to Early Mesozoic mafic–ultramafic complexes from the northern North China Block: constraints on the composition and evolution of the lithospheric mantle. Lithos 110, 229–246.

Zhang, S.H., Zhao, Y., Liu, J.M., Hu, J.M., Song, B., Liu, J., Wu, H., 2010. Geochronology, geochemistry and tectonic setting of the Late Paleozoic–Early Mesozoic magmatism in the northern margin of the North China block: a preliminary review. Acta Petrologica et Mineralogica 29, 824–842 (in Chinese with English abstract).

Zhang, X., Mao, Q., Zhang, H., Zhai, M.G., Yang, Y., Hu, Z., 2011a. Mafic and felsic magma interaction during the construction of high-K calc-alkaline plutons within a metacratonic passive margin: the Early Permian Guyang batholith from the northern North China Craton. Lithos 125, 569–591.

Zhang, X., Wilde, S.A., Zhai, Zhang H., M., 2011b. Early Permian high-K calc-alkaline volcanic rocks from NW Inner Mongolia, North China: geochemistry, origin and tectonic implications. Journal of the Geological Society London 168, 153–171.

Zhang, X., Gao, Y., Wang, Z., Liu, H., Ma, Y., 2012. Carboniferous appinitic intrusions from the northern North China craton: geochemistry, petrogenesis and tectonic implications. Journal of the Geological Society London 169, 337–351.

Zhang, S.H., Zhao, Y., 2013. Mid-crustal emplacement and deformation of plutons in an Andean-style continental arc along the northern margin of the North China block and tectonic implications. Tectonophysics 608, 176–195.

Zhang, S.H., Zhao, Y., Ye, H., Liu, J.M., Hu, Z.C., 2014. Origin and evolution of the Bainaimiao arc belt: implications for crustal growth in the southern Central Asian orogenic belt. Geological Society of America Bulletin 126, 1275–1300.

Zhou, Z.G., Zhang, H.F., Liu, H.L., Liu, C.F., Liu, W.C., 2009. Zircon U–Pb dating of basic intrusions in Siziwangqi area of middle Inner Mongolia, China. Acta Petrologica Sinica 25, 1519–1528 (in Chinese with English abstract).